



**Steel Founders' Society of America
Research Report No. 94B**

**Fatigue and Fracture Toughness
Of Five Carbon or Low Alloy
Cast Steels at Room or Low
Climate Temperature (Part II)**

Published by the
Carbon and Low Alloy Steel Technical Research Committee
Steel Founders' Society of America

DR. JOHN M. SVOBODA
Technical and Research Director

MAY, 1983

**Fatigue and Fracture Toughness of Five Carbon
or Low Alloy Cast Steels at Room
or Low Climatic Temperatures
(Part II)**

By: Ralph L. Stephens

Table of Contents

Chapter	Page
Preface	i
Summary and Conclusions	ii
7 High Cycle Axial Fatigue of Smooth Specimens at Room Temperature and -50°F (-45°C)	1
7.1 Test Procedures	1
7.2 Test Results and Discussion	1
7.3 Summary and Conclusions	3
References	3
8 Threshold, ΔK_{th} , and Near Threshold Fatigue Crack Growth Behavior at Room Temperature and -50°F (-45°C)	4
8.1 Introduction	4
8.2 Test Procedures	4
8.3 Test Results and Discussion	5
8.4 Summary and Conclusions	9
References	9
9 Variable Amplitude Fatigue Crack Initiation and Growth Calculations at Room Temperature and -50°F (-45°C)	10
9.1 Introduction	10
9.2 Mathematical Models	10
9.2.1 Fatigue Crack Initiation	10
9.2.2 Short Crack Growth	11
9.2.3 Long Crack Growth	11
9.3 Comparison of Experimental and Calculated Fatigue Lives	12
9.4 Summary and Conclusions	14
References.....	14
10 Integration of Fatigue and Fracture Behavior	15
10.1 Introduction	15
10.2 Room Temperature.....	18
10.2.1 Monotonic Tensile Test	18
10.2.2 Fracture Toughness	18
10.2.3 Constant Amplitude Axial Fatigue	18
10.2.4 Constant Amplitude Fatigue Crack Growth	19
10.2.5 Variable Amplitude Fatigue	19
10.3 -50°F(-45°C) Temperature	19
10.3.1 Monotonic Tensile Test	19
10.3.2 Fracture Toughness	19
10.3.3 Constant Amplitude Axial Fatigue	20
10.3.4 Constant Amplitude Fatigue Crack Growth.....	20
10.3.5 Variable Amplitude Fatigue	20
10.4 Summary and Conclusions	21

PREFACE

The original SFSA research project 111 (Dec., 1981) was extended in order to complete the needed fatigue properties of five common carbon or low alloy cast steels. The original report was also incomplete, since the variable amplitude fatigue crack initiation and growth calculations could not be properly made without the extended fatigue research. A proper integration of all the fatigue behavior also could not be made without the extension data. This report includes the results of the extended research, the fatigue life calculations, and the integration. This report has been written assuming the reader is well acquainted with the original report of Dec., 1981. Repetition of the first report has been omitted, except some integration has been made for better continuity. The new chapters have been labeled 7 through 10 in order to provide referencing to the previous chapters.

This fatigue research report includes:

Chapter 7: the extension of smooth specimen axial low cycle fatigue behavior from about 10^5 or 10^6 reversals to 2×10^7 reversals at both room temperature and -50°F (-45°C). Specifically, fatigue limits, S_f , and fatigue ratios S_f/S_u for the fully-reversed condition, $R = -1$, were obtained in addition to completing the entire $\epsilon - 2N_f$ curves.

Chapter 8: the extension of region II fatigue crack growth behavior to threshold and near threshold regions with da/dN ranging from about 4×10^{-7} to 4×10^{-9} incycle (10^{-8} to 10^{-10} m/cycle) at room temperature and -50°F (-45°C). Specifically, threshold stress intensity factors, ΔK_{th} , for $R = 0.05$ and $R = 0.5$ were obtained in addition to completing the entire $da/dN - \Delta K$ curves.

Chapter 9: the fatigue crack initiation and fatigue crack growth life calculations for the compact keyhole notch specimens using the T/H and mod T/H variable amplitude load histories at room temperature and -50°F (-45°C).

Chapter 10: the integration of the total fatigue and fracture behavior including fracture toughness, low and high cycle fatigue, fatigue crack growth under constant amplitude loading, and fatigue crack initiation and growth under variable amplitude loading.

Prof. Stephens, his students and his staff are to be commended on a major contribution to the understanding of the behavior of cast steels. The Carbon and Low Alloy Technical Research Committee wishes to express its appreciation on behalf of the Society for this fine work.

Dr. John Svoboda
Technical and Research Director

by direction of the
Carbon and Low Alloy
Technical Research Committee

R. C. Maxton, Chairman

D. C. Harsch
C. Brown
E. J. Lenar
K. Murphy
W. Scott
E.K. Weber
A. K. Zaman

SUMMARY AND CONCLUSIONS

A comprehensive research project to obtain room temperature and low climatic temperature [principally - 50°F (- 45 °C)] fatigue and fracture properties of five representative carbon or low alloy cast steels was performed at The University of Iowa during 1979 to 1982. The five cast steels were SAE 0030, SAE 0050A, C-Mn, Mn-Mo and AISI 8630. The metallurgical structure of the first two steels was ferrite-pearlite while the later three steels were tempered martensite. The ultimate strengths varied from 72 to 166 ksi (496 to 1144 MPa) which indicates a wide range in ultimate strengths. The following fatigue or fracture properties were obtained along with SEM fracto-graphic analysis:

1. Constant amplitude axial smooth specimen low cycle and high cycle fatigue using strain or load control with approximately 10^2 to 2×10^7 reversals to failure.
2. Constant amplitude fatigue crack growth rates from 10^{-4} to 4×10^{-9} in/cycle (2.5×10^{-6} to 10^{-10} m/cycle) which includes the log-log linear region, near threshold and threshold behavior.
3. Variable amplitude fatigue crack initiation and growth behavior using a keyhole notched specimen.
4. Complete Charpy V notch energy and NDT temperatures.
5. Plane stress fracture toughness and R-curves.
6. Plane strain fracture toughness using the J-integral.

In addition to the above, fatigue life calculations were made for the variable amplitude loadings using the constant amplitude fatigue properties and several life prediction models. An integration of the different test results was made and a complete summary of the properties at the two principal test temperatures are given in Tables 10.1 and 10.2.

The monotonic tensile properties and the fracture properties were quite varied for the five cast steels, while the fatigue resistance was somewhat similar. For instance, at room temperature, the smooth specimen fatigue limits varied from 28.5 to 42.4 ksi (196 to 293 MPa) for the five cast steels, the notched fatigue limits (not a requirement of this project) varied from 18 to 21 ksi (124 to 147 MPa), the threshold stress intensity factors for $R = 0$ varied from 7.4 to 9.3 ksi $\sqrt{\text{in}}$ (8.1 to 10.2 MPa $\sqrt{\text{m}}$) and the variable amplitude reversals to several different fatigue criteria varied by factors between 1.6 and 5.3. These are not large differences.

All five cast steels were suitable for room temperature fatigue design situations and can be best ranked in the following general order: 8360, Mn-Mo, C-Mn or 0050A and then 0030. At -50°F (-45°C) the fatigue resistance generally increased for most of the different tests with the cast steels except for 0050A. This steel showed substantial decreases in fatigue crack growth resistance and fracture resistance at this low temperature. The 0050A steel is not recommended for fatigue design situations at this low climatic temperature. The ranking of the four suitable steels for fatigue resistance at -50 °F (-45°C) was: 8630, Mn-Mo, C-Mn and 0030.

The fatigue life calculations were made with procedures developed principally for wrought products and these proved to be quite successful for the five cast steels. Thus it appears that fatigue life predictions of sound machined cast steels can be made in a similar manner commonly used for wrought products.

Many of the cast steel fatigue properties were compared with literature values for wrought steels and were found to be similar to, or better than, wrought steel values. This appears to be a very important aspect and should receive further research.

High Cycle Axial Fatigue of Smooth Specimens at Room Temperature and -50°F (-45°C)

7.1 Test Procedures

High cycle axial fatigue tests were performed in load control with $R = -1$ using the 20 kip (89 kN) closed-loop electrohydraulic test system. Test frequencies were between 23 and 37 Hz and failures ranged from 105 reversals to run-outs at 2×10^7 reversals. Between three and eight smooth specimens were tested in the high cycle region and ten to twelve smooth specimens had previously been tested in the low cycle fatigue region. The same specimen geometry for the low cycle tests were used for the high cycle tests. Specimen geometry is given in Fig. 2.1 and specimen preparation and mounting is given in section 2.1.

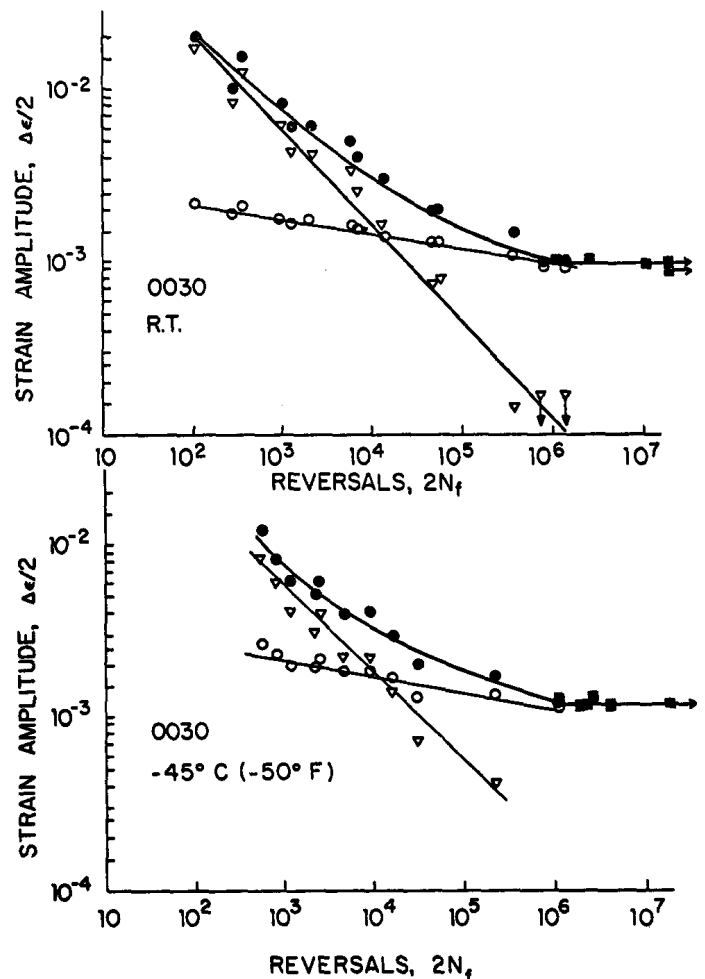
7.2 Test Results and Discussion

Typical high cycle fatigue data are superimposed with the low cycle fatigue data in Figures 7.1 and 7.2. These two Figures are for the two extreme ultimate strength cast steels 0030 and 8630. The solid circles represent total strain amplitudes for the strain controlled low cycle fatigue tests from Figures 2.10 and 2.14, while the solid squares represent total strain amplitudes from the load controlled high cycle fatigue tests. These later strains were calculated by dividing the applied stress amplitude by Young's modulus E , since these tests were run in the elastic region. All five cast steels exhibited typical fatigue limits around 5×10^6 to 10^7 reversals for both room temperature and -50°F (-45°C). Values of the fully-reversed fatigue limits, S_f , were obtained from plots similar to Figures 7.1 and 7.2 for all five cast steels at both test temperatures. These values are given in Table 7.1 along with the fatigue ratios S_f/S_u .

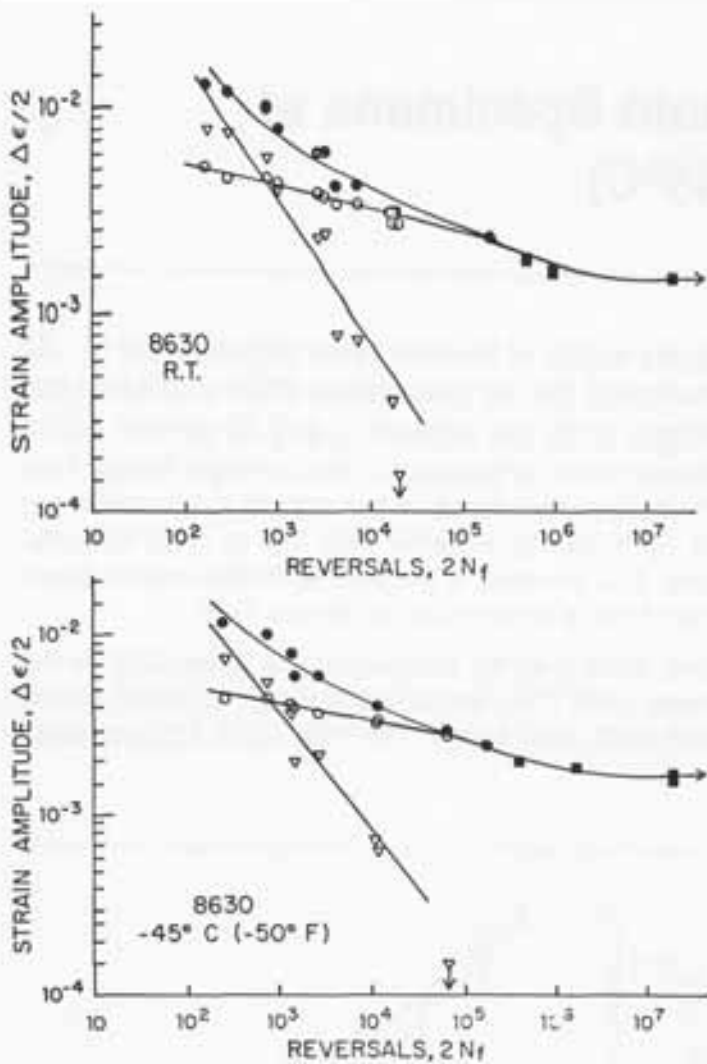
The fatigue curves of Figures 7.1 and 7.2 and the fatigue limits in Table 7.1 do not completely show the effect of temperature on fatigue behavior nor the comparison of the five cast steels at a given temperature. The total strain-life curves have been superimposed in Fig. 7.3 for proper comparison of temperature influence. The solid curves in Fig. 7.3 represent room temperature behavior and the dashed curves are for -50°F (-45°C). Since these are log-log plots, differences between curves are less evident. No specific shape comparison is noted for the five cast

steels except at the high cycle fatigue region ($> 10^5$ reversals), the low temperature strain amplitudes and fatigue limits are between 2 and 25 percent higher than at room temperature. Thus at longer fatigue lives the fatigue resistance of the smooth axial specimens at -50°F (-45°C) is better than that at room temperature. This increase is in agreement with smooth specimen fatigue limits found by others. [1-3]

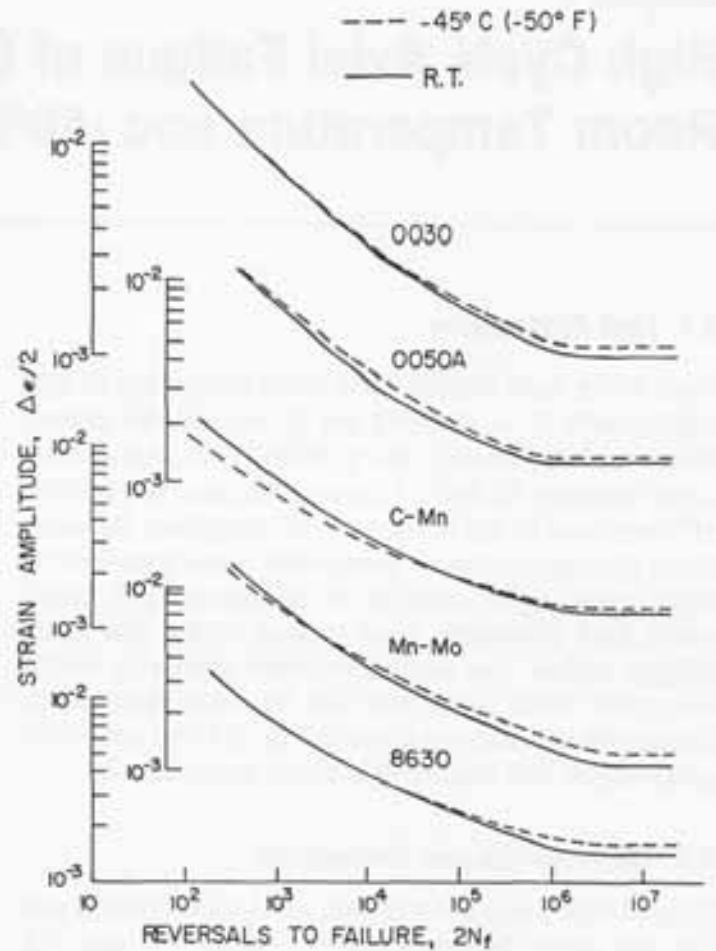
The -50°F (-45°C) temperature is essentially in the lower shelf CVN temperature range for 0030, 0050A and 8630 cast steels. The high cycle fatigue resist-



7.1 Axial fatigue behavior for 0030 cast steel at room temperature and -45°C (-50°F).



7.2 Axial fatigue behavior for 8630 cast steel at room temperature and -45°C (-50°F).



7.3 Influence of -45°C (-50°F) temperature on axial fatigue behavior.

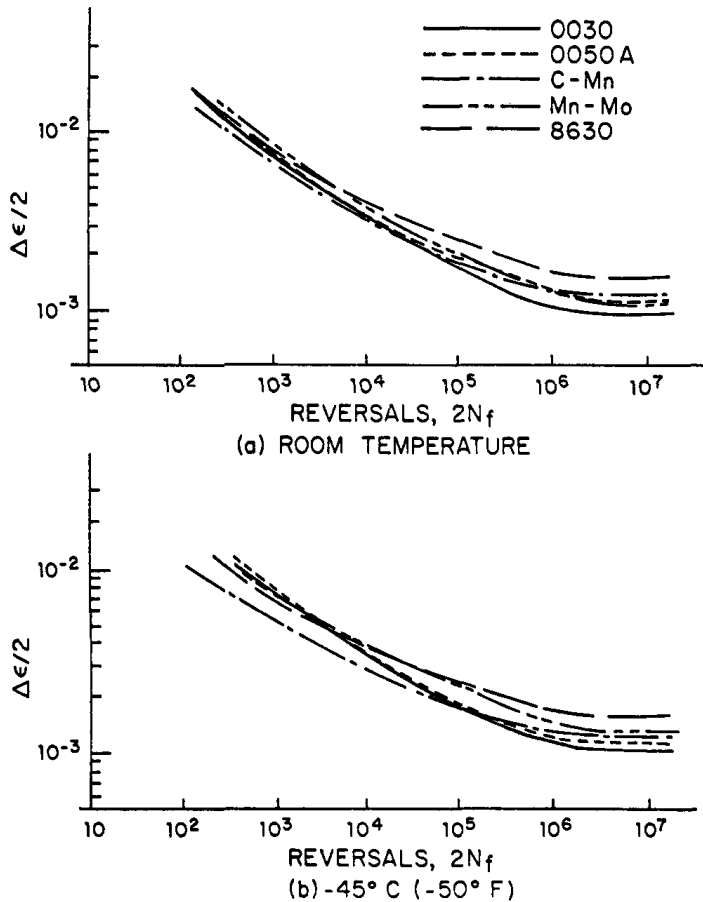
Table 7.1. Cast Steel Fully-Reversed Unnotched Axial Fatigue Limits and Fatigue Ratios.

Material	Room Temperature		-45°C (-50°F)	
	Fatigue Limit S_f ksi (MPa)	Fatigue Ratio S_f/S_u	Fatigue Limit S_f ksi (MPa)	Fatigue Ratio S_f/S_u
0030	28.5 (196)	.40	35 (241)	.44
0050A	34.4 (237)	.30	35.2 (243)	.29
C-Mn	36 (248)	.42	37 (255)	.42
Mn-Mo	33.7 (232)	.33	39 (269)	.35
8630	42.4 (293)	.26	53 (365)	.31

ance obtained from the smooth axial specimens, however, was not degraded at this low temperature. Thus detrimental changes in high cycle fatigue crack initiation and propagation mechanisms at low temperature were not related to the impact CVN lower shelf region.

The total strain-life curves have been superimposed in Fig. 7.4 for each of the two test temperatures in order to better compare fatigue resistance of the five cast

steels. The curves tend to band together at short lives (except C-Mn at low temperature) and then tend to diverge in the high cycle region. From Table 7.1 and from Fig. 7.4, the fatigue limits, S_f , vary from 28.5 to 42.4 ksi (196 to 293 MPa) at room temperature and from 35 to 53 ksi (241 to 365 MPa) at -50°F (-45°C). This range is about a factor of 1.5 for both temperatures which is somewhat less than the factor of over 2.0 for the range of ultimate tensile strengths. For



7.4 Comparison of five cast steels fatigue behavior at room temperature and -45°C (-50°F).

both temperatures the 0030 steel had the lowest value of S_f and the 8630 steel had the highest value.

The fatigue ratios S_f/S_u are given in Table 7.1 and they varied from 0.26 to 0.42 at room temperature and 0.29 to 0.44 at -45°C (-50°F). These ratios are lower than the approximate value of 1/2 often reported for

steel bend specimens. The fatigue ratios for axial specimens, however, are consistently 15 to 25 percent lower than for rotating bend specimens. This would yield axial fatigue ratios between about 0.35 and .45 for most steels. Thus the 0050A and 8630 steels appear to have a somewhat low fatigue ratio compared to the other steels.

7.3 Summary and Conclusions

1. Fully reversed axial fatigue limits were obtained for the five cast steels at room temperature and -50°F (-45°C). Values of S_f varied from 28.5 to 42.4 ksi (196 to 283 MPa) at room temperature and from 35 to 53 ksi (241 to 365 MPa) at -50°F (-45°C). These values ranged within a factor of 1.5 for a given temperature.
2. Fatigue ratios defined by S_f/S_u ranged from 0.26 to 0.42 at room temperature and from 0.29 to 0.44 at -50°F (-45°C). These values are for axial loads which are usually 15 to 25 percent lower than for rotating bending. Values for 0050A and 8630 cast steels appear to be lower than that found in many wrought steels.
3. S_f at -50°F (-45°C) were 2 to 25 percent higher than at room temperature even though the low temperature was essentially in the lower shelf CVN region for three of the five cast steels.

References

1. P.G. Forrest, Fatigue of Metals, Pergamon Press, New York, 1962.
2. J.Y. Mann, Fatigue of Materials, Melbourne University Press, Melbourne, Australia, 1967.
3. R.I. Stephens, J.H. Chung and G. Glinka, "Low Temperature Fatigue Behavior of Steels - A Review", paper No. 790517, April 1979, SAE Transactions, Vol. 88, 1980, p. 1892.

Threshold, ΔK_{th} , and Near Threshold Fatigue Crack

Growth Behavior at Room Temperature and -50°F (-45°C)

8.1 Introduction

Constant amplitude fatigue crack growth rate (FCGR) behavior above approximately 4×10^{-7} in/cycle (10^{-8} m/cycle) were given in Chapter 3 for the five cast steels with $R \approx 0$ and $1/2$ for both room temperature and -50°F (-45°C). This chapter contains FCGR behavior for rates between 4×10^{-7} and 4×10^{-9} in/cycle (10^{-8} and 10^{-10} m/cycle) for the five cast steels with $R = 0.05$ (≈ 0) and 0.5 at both room temperature and -50°F (-45°C). This extension data plus the original data provide the complete da/dN versus ΔK curves of regions I and II of the usual sigmoidal curve. Region I is often called the near threshold and threshold region. The threshold stress intensity factor, ΔK_{th} , can be defined as the limiting value of ΔK where crack growth does not occur. A more realistic functional definition by Bucci, given in the ASTM proposed test standard (1), implies fatigue crack growth rates equal to 4×10^{-9} in/cycle (10^{-10} m/cycle) can be used to define ΔK_{th} . This definition was used in this research.

8.2 Test Procedures

To obtain the FCGR data near the threshold region without any retardation effect from load interactions, the ASTM proposed standard suggests two methods. One is a continuous load shedding method using computer control of the test system and the other is an incremental load shedding method used until the threshold value is obtained, at which time the load is then maintained at a constant amplitude (1). The incremental load shedding method was used in this research because of the test machine capabilities.

The chevron test specimen for this region I FCGR behavior had the same configuration as that for region II and is shown in Fig. 3.1. The thickness was 0.324 in (8.2 mm). The tests were run with the 20 kip (89 kN) closed-loop electrohydraulic test system using a 2 kip (89 kN) load cell. The low temperature tests were run in an automated CO_2 temperature chamber. The crack growth was measured with a traveling telescope with a least reading of 0.0004 in (0.01 mm). Tests were run 24 hours per day in load control at 30-40 Hz. Each test took about 4 to 5 continuous days.

Precracking from the chevron machined notch was done using the procedure recommended in ASTM standard E647 (2) which is the recommended procedure in the proposed ASTM ΔK_{th} standard (1). The precracking was done with 10 percent load decreases and crack growth of between .02 to .04 in (.5 to 1 mm) for each load level. To obtain the FCGR below 4×10^{-7} in/cycle (10^{-8} m/cycle) the load shedding was reduced from 10 percent at the beginning to 2 to 3 percent near ΔK_{th} . The percent decrease was lowered as the FCGR decreased. The ASTM proposal (1) requires a minimum crack growth of 0.04 in (1.0 mm) with a 10 percent drop of ΔK or 0.025 in (0.63 mm) with a 5 percent drop of ΔK . To minimize the testing time, $d(\Delta K)/\Delta K$ and Δa values were specifically reduced as follows where $d(\Delta K)$ is the increment of ΔK at each step and Δa is the crack growth at each step:

- (1) For da/dN between 4×10^{-7} and 4×10^{-8} in/cycle (10^{-8} and 10^{-9} m/cycle) $d(\Delta K)/\Delta K$ was between -0.08 and -0.05 and Δa was between 0.02 and 0.04 in (0.5 and 1 mm).
- (2) For da/dN between 4×10^{-8} and 4×10^{-9} in/cycle (10^{-9} and 10^{-10} m/cycle) $d(\Delta K)/\Delta K$ was between -0.06 and -0.03 and Δa was between 0.01 and 0.02 in (0.25 and 0.5 mm).

For the $R = 1/2$ tests, K_{max} and K_{min} were reduced in the same manner.

A typical load shedding procedure is shown in Fig. 8.1. In the figure, $d(\Delta K)/da$ is the slope of nominal ΔK curve. At each step of the load, the FCGR was calculated and compared with the value of the previous step. If the FCGR showed an irregular high or low value, $d(\Delta K)/\Delta K$ for the next step was reduced a few percent more or less. The actual $d(\Delta K)/\Delta K$ at the instant of load drop shows a few percent higher than $\Delta P/P$ due to the increase of ΔK value as $f(a, W)$ from equation 3.2 increases.

To make sure fatigue crack growth retardation did not occur in the decreasing ΔK tests, an increasing ΔK test was often run after the required ΔK_{th} was obtained. To reduce the time for these tests, the loads were increased 2 to 3 percent and the FCGR was measured during 0.01 to 0.02 in (0.25 to 0.5 mm) of crack growth at each step. For ΔK decreasing tests, retardation

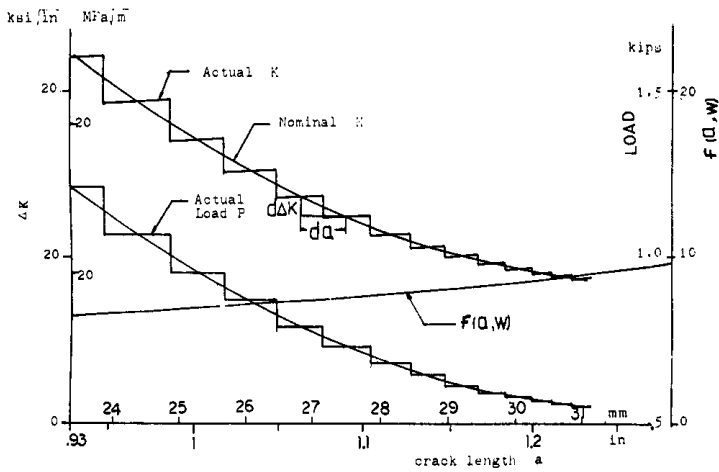


Figure 8.1 Load shedding method for near threshold crack growth test.

may occur in the monotonic plastic zone size r_y . The FCGR thus was checked from the point where the new monotonic plastic zone passed over the previous plastic zone at each load step. The plastic zone size was calculated under plane stress conditions. 8630 cast steel was used to check for possible retardation during the decreasing step test. For the first test, the average crack growth rates and the crack growth rates free from retardation effects were measured. The crack growth rates during the ΔK increasing test were also measured. To verify the first test result, a duplicate test was done and the average crack growth rate at each step was checked. As the comparison of the three different methods showed no significant differences, all of the following tests were done only with the decreasing test except when the FCGR showed inconsistent behavior. In this case the increasing test was done to assure the data obtained during the decreasing test were correct. The ΔK increasing tests were done for 8630 at room temperature and -50°F (-45°C) for both $R = 0.05$ and $R = 1/2$, 0050A at room temperature for both $R = 0.05$ and $R = 1/2$ and Mn-Mo cast steel at -50°F (-45°C) for both $R = 0.05$ and $1/2$. These results were very consistent with decreasing ΔK results.

8.3 Test Results and Discussion

The crack growth rate da/dN was calculated with the secant method by averaging the crack growth increment over the elapsed number of cycles ΔN_i . The ΔK_i values were calculated at the center of the crack increment with equation 3.2. The crack lengths measured at one side of the surfaces were corrected from the measurements of crack lengths at both sides and the curvature of the crack tip, by taking the

average crack lengths after the test was over.

Both region I and region II (from chapter 3) data are plotted together for the five cast steels at both temperatures in Figures 8.2 to 8.11. The transition regions are connected very well even though the tests were done completely separate for region I and II. Each figure has both $R \approx 0$ and $R = 1/2$ data plotted for a given cast steel and test temperature. Figures 8.2 to 8.6 are for room temperatures and Figures 8.7 to 8.11 are for -50°F (-45°C).

Generally it is hard to obtain data evenly distributed in the 4×10^{-8} to 4×10^{-9} in/cycle (10^{-9} to 10^{-10} m/cycle) region because the FCGR near the threshold drops sharply. Bucci (1) recommended a straight line regression analysis of at least five data points in the 4×10^{-8} to 4×10^{-9} in/cycle (10^{-9} to 10^{-10} m/cycle) region to decide the threshold stress intensity factor range ΔK_{th} . This method seems unreasonable for these cast steels as the crack growth rate curves show knees in that region and a sudden drop near the threshold level. In this research the threshold values were also determined from a median curve drawn by visual examination in Figures 8.2 to 8.11. If there were no available data points lower than 8×10^{-9} in/cycle (2×10^{-10} m/cycle) the median curve was extended from

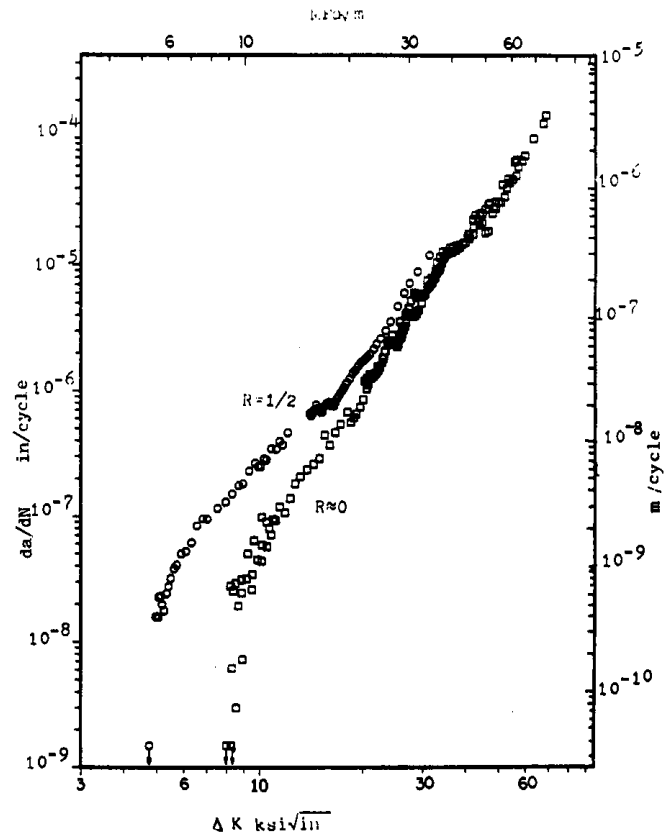


Figure 8.2. Composition da/dN versus ΔK for $R \approx 0$ and $R = 1/2$ for 0030 cast steel at room temperature.

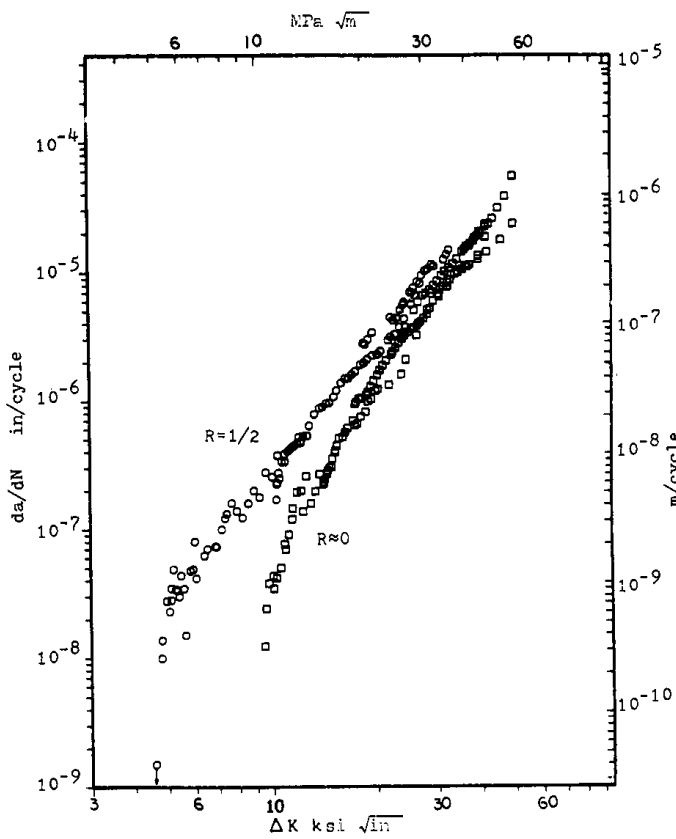


Figure 8.3 Composite da/dN versus ΔK for $R \approx 0$ and $R = 1/2$ for 0050A cast steel at room temperature.

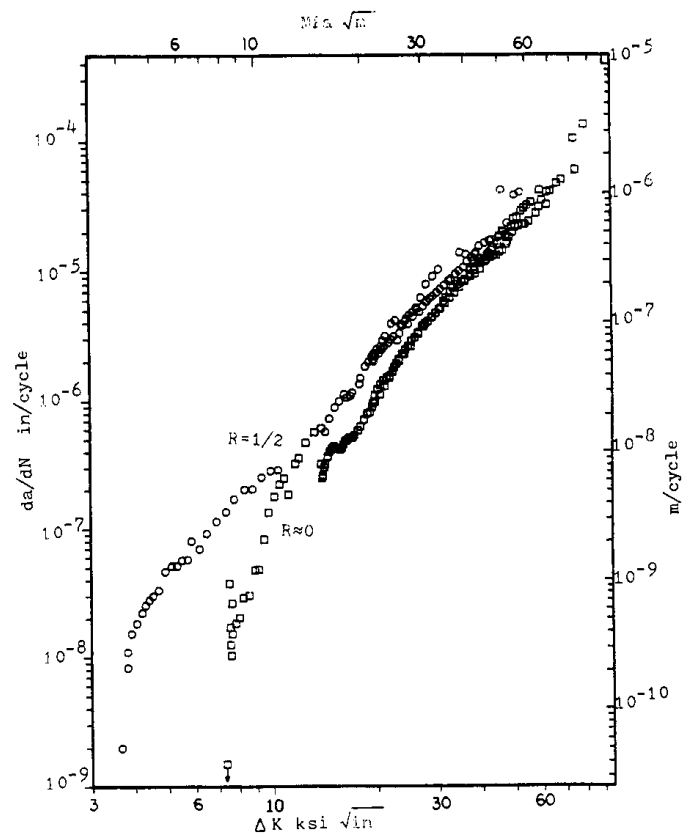


Figure 8.5 Composite da/dN versus ΔK for $R \approx 0$ and $R = 1/2$ for Mn-Mo cast steel at room temperature.

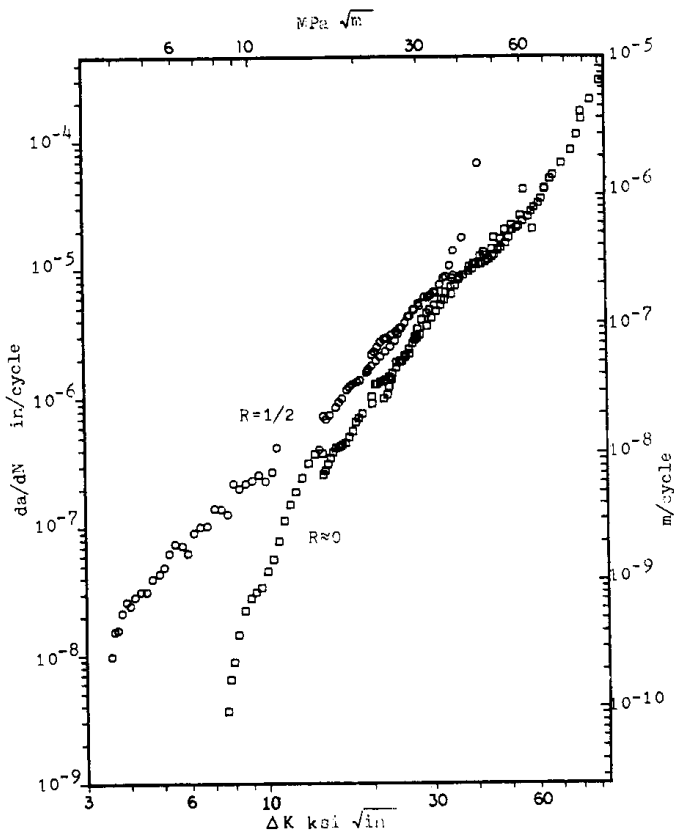


Figure 8.4 Composite da/dN versus ΔK for $R \approx 0$ and $R = 1/2$ for C-Mn cast steel at room temperature.

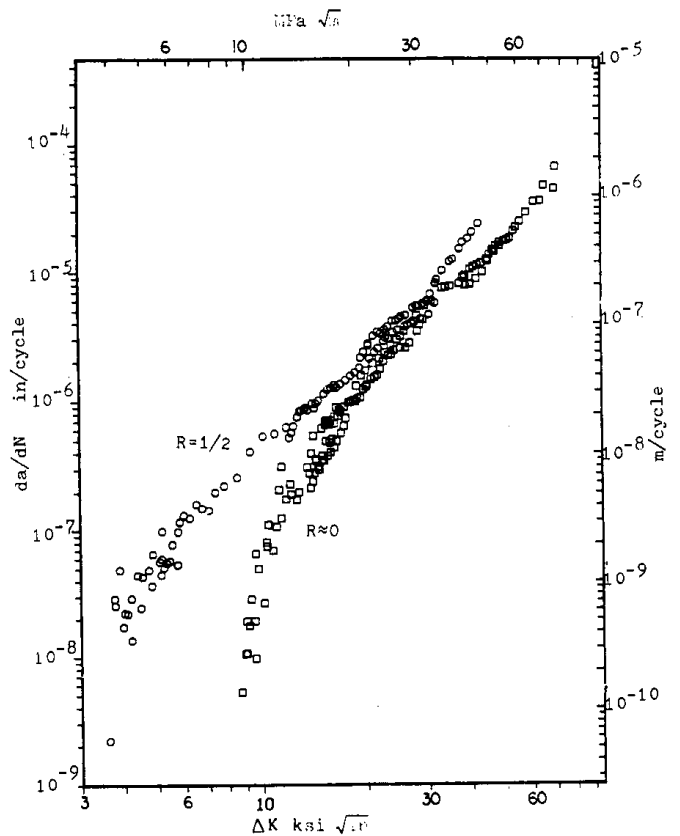


Figure 8.6 Composite da/dN versus ΔK for $R \approx 0$ and $R = 1/2$ for 8630 cast steel at room temperature.

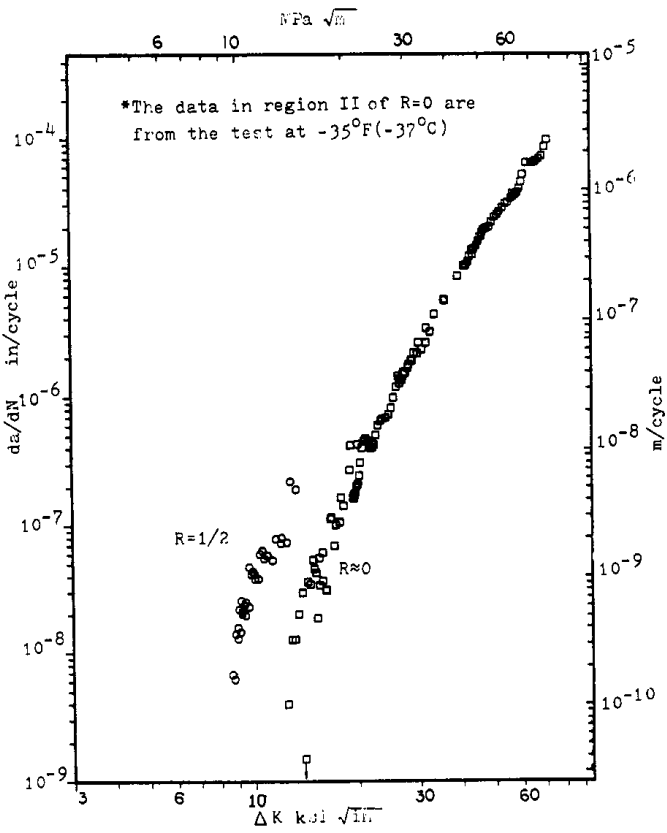


Figure 8.7 Composite da/dN versus ΔK for $R \approx 0$ and $R = 1/2$ for 0030 cast steel at -50°F (-45°C).

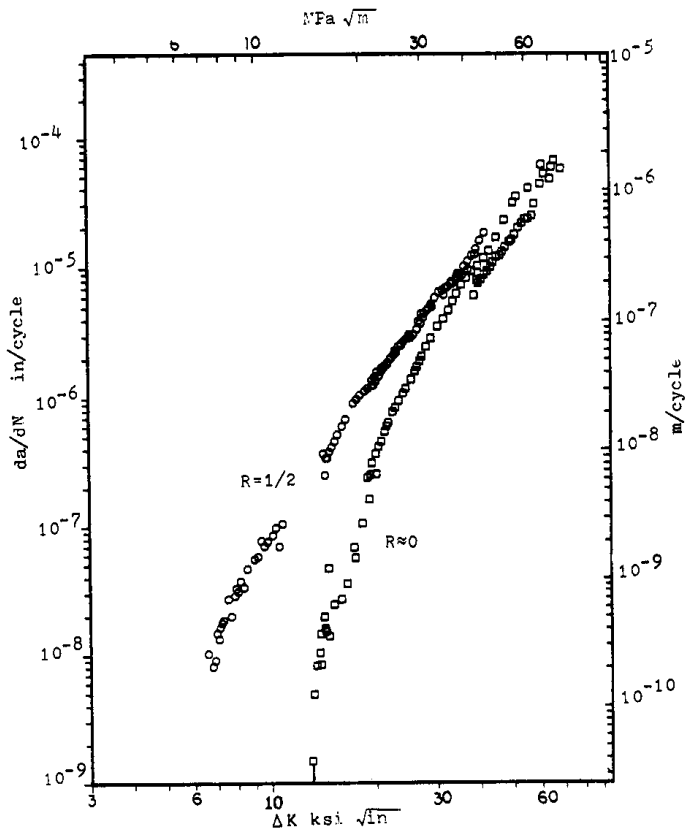


Figure 8.9 Composite da/dN versus ΔK for $R \approx 0$ and $R = 1/2$ for C-Mn cast steel at -50°F (-45°C).

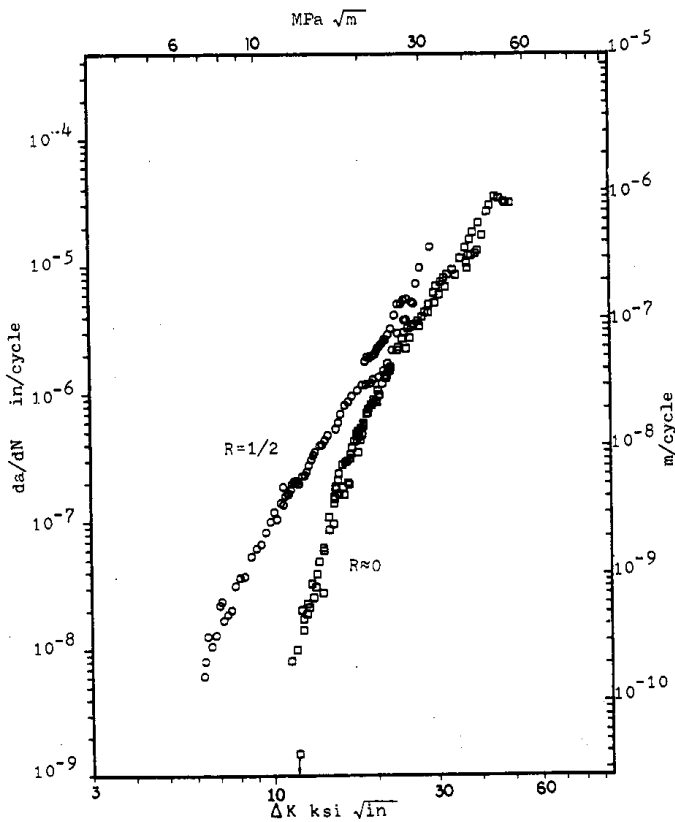


Figure 8.8 Composite da/dN versus ΔK for $R \approx 0$ and $R = 1/2$ for 0050A cast steel at -50°F (-45°C).

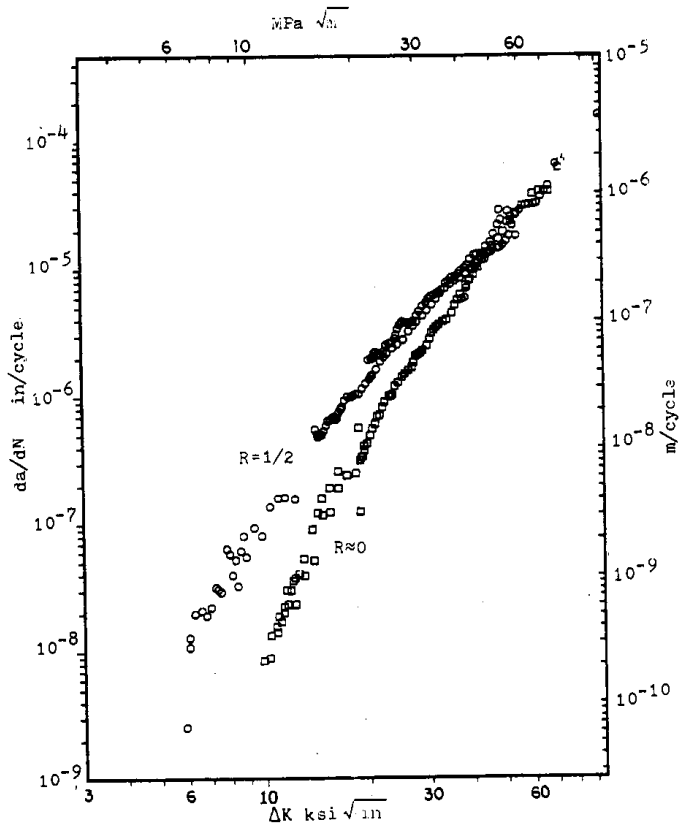


Figure 8.10 Composite da/dN versus ΔK for $R \approx 0$ and $R = 1/2$ for Mn-Mo cast steel at -50°F (-45°C).

were obtained for da/dN equal to 4×10^{-9} in/cycle (10^{-10} m/cycle) as suggested in the proposed ASTM standard (1).

The values of ΔK_{th} are given in Table 8.1 for the median visual procedure and in Table 8.2 for the linear regression procedure. The median visual procedure values (Table 8.1) are taken as the most meaningful and realistic values and should be used for these five cast steels. ΔK_{th} for the five cast steels at room temperature with $R = 0.05$ ranged from 7.4 to 9.3 ksi \sqrt{in} (8.1 to 10.1 MPa \sqrt{m}) and at $R = 1/2$ from, 3.5 to 4.8 ksi \sqrt{in} (3.8 to 5.2 MPa \sqrt{m}). Tanaka (3) has shown that ΔK_{th} at room temperature with $R \approx 0$ for 73 wrought steels ranged from 2.7 to 14 ksi \sqrt{in} (3 to 15 MPa \sqrt{m}); but only 22 of these 73 wrought steels had ΔK_{th} values equal to or higher than the five cast steels. This is a very positive indication for cast steels which deserves additional comparative investigation.

The ΔK_{th} values showed no consistent correlation with other properties such as yield strength, ultimate strength or fatigue limit. At $R = 1/2$ for both temperatures, the ΔK_{th} values generally decreased to about 50 percent of the values at $R = 0.05$ (actual percentage varied from 42 to 58) which indicates the importance of apparent mean stress. This behavior is consistent with many materials and can be closely associated with crack closure. Crack opening and closing displacements were measured during region I FCGR tests for 0030 at both temperatures and for C-Mn at $-50^\circ F$ ($-45^\circ C$) with ΔK equal to 1 to 2 times ΔK_{th} . The crack opening load could be obtained from the

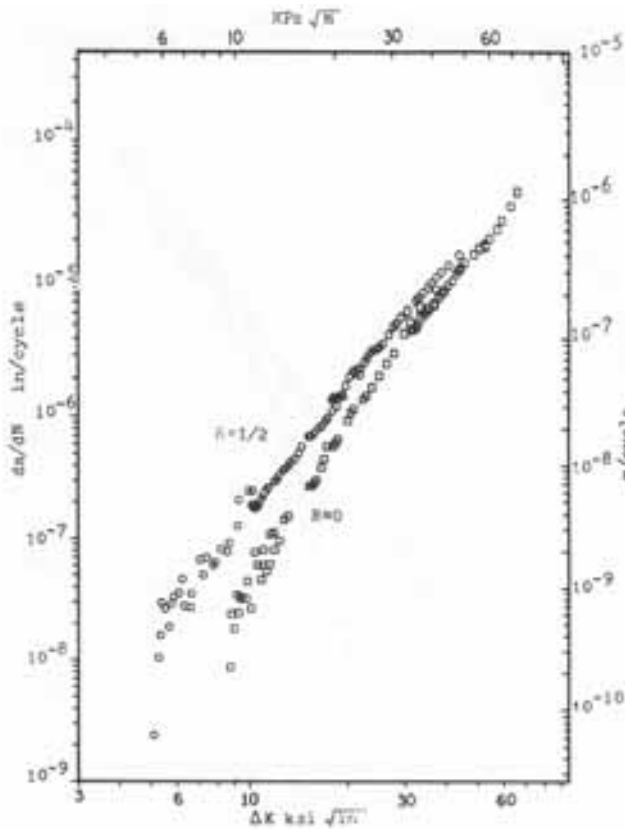


Figure 8.11 Composite da/dN versus ΔK for $R=0$ and $R=1/2$ for 8630 cast steel at $-50^\circ F$ ($-45^\circ C$).

the knee region along the slope and the threshold stress intensity factor was taken at 4×10^{-9} in/cycle (10^{-10} m/cycle) growth rate. Thus all ΔK_{th} values

Table 8.1. ΔK_{th} for Five Cast Steels Using Median Visual Examination.

Material	R = 0.05		R = 1/2	
	Room Temperature MPa \sqrt{m} (ksi \sqrt{in})	-45°C (-50°F) MPa \sqrt{m} (ksi \sqrt{in})	Room Temperature MPa \sqrt{m} (ksi \sqrt{in})	-45°C (-50°F) MPa \sqrt{m} (ksi \sqrt{in})
0030	9.1 (8.3)	14.2 (12.9)	5.3 (4.8)	9.3 (8.5)
0050A	10.2 (9.3)	12.3 (11.2)	5.2 (4.7)	6.8 (6.2)
C-Mn	8.3 (7.6)	14.4 (13.1)	3.9 (3.5)	7.1 (6.5)
Mn-Mo	8.1 (7.4)	10.7 (9.7)	4.1 (3.7)	6.5 (5.9)
8630	9.4 (8.6)	9.4 (8.6)	4.1 (3.7)	5.7 (5.2)

Table 8.2. ΔK_{th} for Five Cast Steels Using Linear Regression.

Material	R = 0.05		R = 1/2	
	Room Temperature MPa \sqrt{m} (ksi \sqrt{in})	-45°C (-50°F) MPa \sqrt{m} (ksi \sqrt{in})	Room Temperature MPa \sqrt{m} (ksi \sqrt{in})	-45°C (-50°F) MPa \sqrt{m} (ksi \sqrt{in})
0030	9.4 (8.6)	14.0 (12.8)	5.6 (5.1)	8.8 (8.1)
0050A	9.3 (8.5)	12.0 (11.0)	5.5 (5.0)	6.0 (5.5)
C-Mn	8.1 (7.4)	14.0 (12.9)	2.8 (2.6)	6.3 (5.8)
Mn-Mo	7.6 (7.0)	9.4 (8.6)	3.8 (3.5)	5.6 (5.1)
8630	8.5 (7.8)	7.2 (6.6)	3.3 (3.0)	4.7 (4.3)

load versus crack opening displacement curves. The loading and unloading curves showed essentially no difference between the crack opening and closing loads. The crack opening or closure loads were observed to be approximately 0.5 P_{max} (actual values were between .45 and .55). These values thus indicate that mean stress influence is closely related to crack closure at both room and low temperature. This concept is also reinforced by the greater amount of fretting often found on the fracture surface for $R = 0.05$ tests compared to that for $R = 1/2$ tests.

At - 50 °F (- 45 °C), ΔK_{th} values increased by 20 to 90 percent compared to room temperature values except for 8630 with $R = 0.05$ which showed no change. 0030 and C-Mn which are two of the lower strength cast steels showed the greatest increases at - 50°F (-45°C) for both R ratios. This general increase in ΔK_{th} at - 50 °F (- 45 °C) is consistent with the general increases reported in Chapter 3 for region II FCGR behavior. Since - 50 °F (- 45 °C) is essentially in the lower shelf CVN region for 0030, 0050A, and 8630 steels, this again indicates that operating temperatures in or above the lower shelf CVN region can yield adequate FCGR resistance.

8.4 Summary and Conclusions

1. ΔK_{th} values were obtained at room temperature and -50°F (-45°C) with $R = 0.05$ and $1/2$ for the five cast steels using a load shedding technique. ΔK_{th} was defined as ΔK when da/dN was 4×10^{-9} in/cycle (10^{-10} m/cycle). A median visual curve better represented ΔK_{th} than a suggested linear regression curve due to substantial curvature in da/dN versus ΔK around 4×10^{-8} in/cycle (10^{-9} m/cycle).
2. ΔK_{th} values at room temperature ranged from 7.4 to 9.3 ksi $\sqrt{\text{in}}$ (8.1 to 10.1 MPa $\sqrt{\text{m}}$) for $R = 0.05$ and from 3.5 to 4.8 ksi $\sqrt{\text{in}}$ (3.8 to 5.2 MPa $\sqrt{\text{m}}$) for $R = 1/2$ for the five cast steels. The $R \approx 0$ values were equal to or better than 50 out of 72 values reported in the literature for wrought steels. This suggests that a further comparative study of wrought and cast steel threshold levels is desirable.
3. ΔK_{th} at $R = 1/2$ was approximately 50 percent of ΔK_{th} at $R = 0.05$. This substantial mean stress effect can be related to crack closure since both crack opening and closure loads were approximately 50 percent of K_{max} for the few tests where these loads were measured.
4. ΔK_{th} values were not related to S_y , S_u nor S_f .
5. At - 50 °F (- 45 °C), ΔK_{th} values increased from 0 to 90 percent compared to values at room temperature. These increases occurred despite the fact that three of the steels at the low temperature were essentially in the lower shelf CVN region.

References

1. R.J. Bucci, "Development of a Proposed Standard Practice for Near Threshold Fatigue Crack Growth Measurement", in Fatigue Crack Growth Measurement and Data Analysis, ASTM STP 738, 1981, p, 5.
2. "Tentative Test Method for Constant Amplitude Fatigue Crack Growth Rates Above 10^{-8} m/cycle", ASTM Annual Book of Standards, Part 10, E647, 1979.
3. K. Tanaka, "A Correlation of ΔK_{th} Values With the Exponent, m , in the Equation of Fatigue Crack Growth for Various Steels", International Journal of Fracture, Vol. 15, No. 1, February, 1979, p. 57.

Variable Amplitude Fatigue Crack Initiation and Growth Calculations at Room Temperature and -50°F (-45°C)

9.1 Introduction

Chapter 4 provided fatigue test results using a keyhole specimen with the T/H and mod T/H variable amplitude load spectra for the five cast steels at room temperature and three low temperatures. Fatigue life calculations for only the room temperature and -50°F (-45°C) tests are given in this chapter. These calculations were made using constant amplitude material properties for the five cast steels as given in chapters 1, 2, 3, 5, 7 and 8 along with mathematical models. The models used in the calculations include both original ideas, models previously published by others, and modifications of these previously published models. The previously published models have principally been used for wrought products and thus, it was not entirely clear a priori whether these models could be suited for cast steel life calculations.

The fatigue life calculations of the keyhole specimens were separated into three major categories as follows:

1. Fatigue crack initiation life with cracks growing to a size equal to an equivalent characteristic length α_{eq} . This characteristic length is quite small with resultant values ranging from 0.01 to 0.027 in (.25 to .69 mm) for the five cast steels.
2. Short crack fatigue crack growth under the influence of the keyhole notch. This region involved fatigue crack growth from α_{eq} to a small region beyond α_{eq} as determined by crack initiation damage from category 1.
3. Long fatigue crack growth, which follows category 2, which is not under the influence of the keyhole notch.

The sum of these three fatigue life calculations represent the total fatigue life of the keyhole specimen. In general, each of the three regions contributed significantly to the total life calculations. In some particular cases, however, a given category may have contributed only a small amount to the total life calculations.

The mathematical models developed, modified and used in these fatigue life calculations are quite com-

plex and involve extensive computer calculations and computer time. It is beyond the scope of this chapter to develop and describe them in detail. For specific details and development, the reader is referred to the Ph.D. thesis of S.G. Lee (1) who did this phase of the research. This chapter however, does provide a brief qualitative description of the modeling and the calculation procedures. Many of the quantitative life calculations from S.G. Lee's Ph.D. thesis are compared with experimental results in this chapter.

Material properties used in these calculations include:

From Chapter 1

E - Young's Modulus
 S_y - Monotonic yield strength
 ν - Poisson's ratio

From Chapter 2

K' - Cyclic strength coefficient
 n' - Cyclic strength exponent
 S'_y - Cyclic yield strength
 b - Fatigue strength exponent
 c - Fatigue ductility exponent
 σ'_f - Fatigue strength coefficient
 ϵ'_f - Fatigue ductility coefficient

From Chapter 3

A - Fatigue crack growth rate coefficient
 n - Fatigue crack growth rate exponent

From Chapter 5

K_e - Elastic fracture thoroughness

From Chapter 7

S_f - Fully-reversed fatigue limit

From Chapter 8

ΔK_{th} - Threshold stress intensity factor range

9.2 Mathematical Models

9.2.1 Fatigue Crack Initiation

1. The cyclic stress-strain equations using the incremental step method (linearly elementized into ten segments) were used to describe the elastic-plastic behavior at the equivalent characteristic length, α_{eq} , up to $\epsilon = 0.016$. After this strain, a

- zero strain hardening exponent was assumed.
2. The low cycle fatigue equations were used to relate strain ranges with cycles to "failure".
 3. K_f for the keyhole notch was determined using FEM.
 4. K_f values for the keyhole specimen were calculated from experimental K_f values determined from center notched axial fatigue specimens which were designed to have similar σ_{max} and average stress gradients over an equivalent characteristic length α_{eq} .
 5. α_{eq} was assumed to be a material constant and was obtained from unnotched and notched fatigue limits and the von Mises criteria.
 6. Cycle counting was done using the Rainflow counting method.
 7. The Palmgren-Minor linear damage rule was used for adding damage per cycle.
 8. Damage was determined at the equivalent characteristic length α_{eq} .
 9. α_{eq} at -50°F (-45°C) was assumed to be similar to α_{eq} at room temperature and thus the room temperature values were used for the low temperature. Likewise, K_f at -50°F (-45°C) was assumed to be the same as at room temperature.
 10. Equivalent stresses and strains, σ_{eq} and ϵ_{eq} , were used at α_{eq} from the von Mises criteria.
 11. Modified Neuber's rule at α_{eq} was used in one set of calculations and an elastic-plastic FEM load versus strain analysis at α_{eq} was used for a second set of calculations.
 12. Mean stresses were handled with modified Neuber's rule by replacing σ'_f in the low cycle fatigue equation with $\sigma'_f - \sigma_m$ and using a simple equation derived by Landgraf.
 13. Crack initiation was assumed complete when the crack had grown to a length equal to α_{eq} .
 14. Crack initiation calculations using the above, were computerized and solved. These were compared with experimental crack initiation lives (crack growth to α_{eq}) obtained by interpolating monitored crack growth results.

9.2.2 Short Crack Growth

1. The short crack was defined from α_{eq} to a bounded distance during which the accumulated damage during crack initiation is considered to be significant.
2. The FCGR in this damaged region was assumed to be greater than in the undamaged region.
3. An exponential equivalent strain distribution was determined in the short crack region using the

elastic-plastic FEM from the crack initiation calculations. The equivalent strain range distribution for the maximum load range of a loading spectrum was calculated and the damaged zone boundary was determined at the point where the strain range is equal to the fatigue limit.

4. The damage for all the load cycles counted by the rainflow counting method were added until the damage in the equivalent characteristic length reached 1.
5. The damage distribution in the damaged zone decreased logarithmically with the distance from the equivalent characteristic length.
6. The crack growth rates in the damaged zone were assumed to be increased by a factor of $1/(1 - D[x])$ compared to the long crack growth rates.

9.2.3 Long Crack Growth

1. The long crack fatigue crack growth life was calculated using crack closure concepts with and without interaction effects. For the interaction calculations, the crack opening model for block loadings by Sunder was modified and used to consider transient effects. Here crack opening loads changed in an exponential manner for the high-low or low-high block loadings.
2. The interaction effects on the crack opening loads for the variable loadings were divided into long and short term interactions. For the long term effect, the crack opening load was controlled by the dominant monotonic plastic zone size, and for the short term effect, the difference between the current crack opening load and the constant amplitude crack opening load was reduced in the same way as the long term interaction.
3. The crack opening load for a compressive load was assumed to be the same as that of constant amplitude loading with the same R ratio.
4. In the linear crack growth model, the crack opening load for each loading was calculated using Newman's crack opening loads for various R ratios.
5. The crack growth for every loading reversal was calculated with a modified form of Newman's effective stress intensity factor equation.
6. ΔK_{th} for different R ratios were estimated using an equation from Klesnil and Lukas. These values were used to eliminate reversals that did not cause crack growth.
7. The crack was assumed to grow until the maximum stress intensity factor reached the elastic fracture toughness K_{e} .

9.3 Comparison of Experimental and Calculated Fatigue Lives

The variable amplitude fatigue tests using the T/H and mod T/H history and the keyhole compact specimen at room temperature and -50°F (-45°C) included two or three different peak loads for all five cast steels. In general, tests were duplicated and between 54 and 2746 blocks to final fracture occurred for the entire program. This range of blocks to fracture was a factor of about 50 to 1. The comparison of the number of experimental blocks, for a particular criteria, with the number of calculated blocks are given on log-log coordinates in Figures 9.1 to 9.6 for room temperature and in Figures 9.7 and 9.8 for -50°F (-45°C). The experimental results in these figures include all replica tests. Only general trends are discussed in this chapter, and the reader is referred to reference 1 for more details.

The room temperature crack initiation lives using modified Neuber's rule and the FEM load-strain model are shown in Figures 9.1 and 9.2 respectively. The two extreme scatter band lines are for factors of ± 4 . The calculated lives in Figure 9.1 are between factors of $+7$ and -4 where the positive sign means a conservative calculation. Except for 0030 and 8630

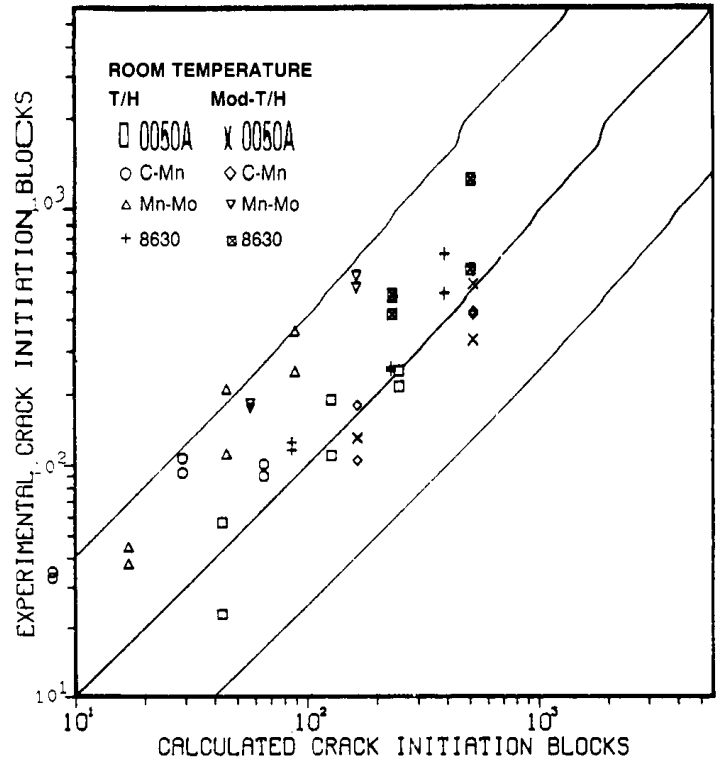
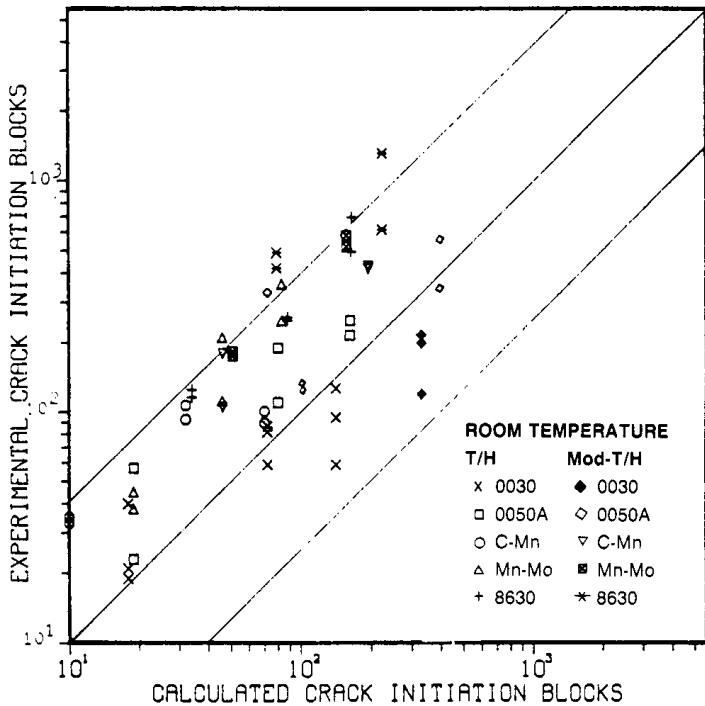


Figure 9.2 Experimental and calculated crack initiation lives using FEM load-strain analysis at room temperature.



9.1 Experimental and calculated crack initiation lives using modified Neuber's rule with incremental stress-strain data at room temperature.

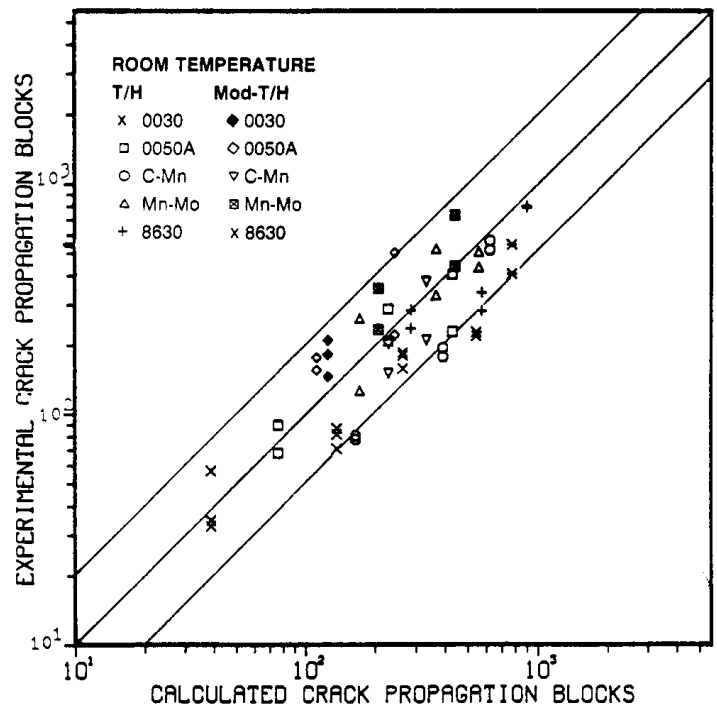


Figure 9.3. Experimental and calculated crack growth lives using interaction model at room temperature.

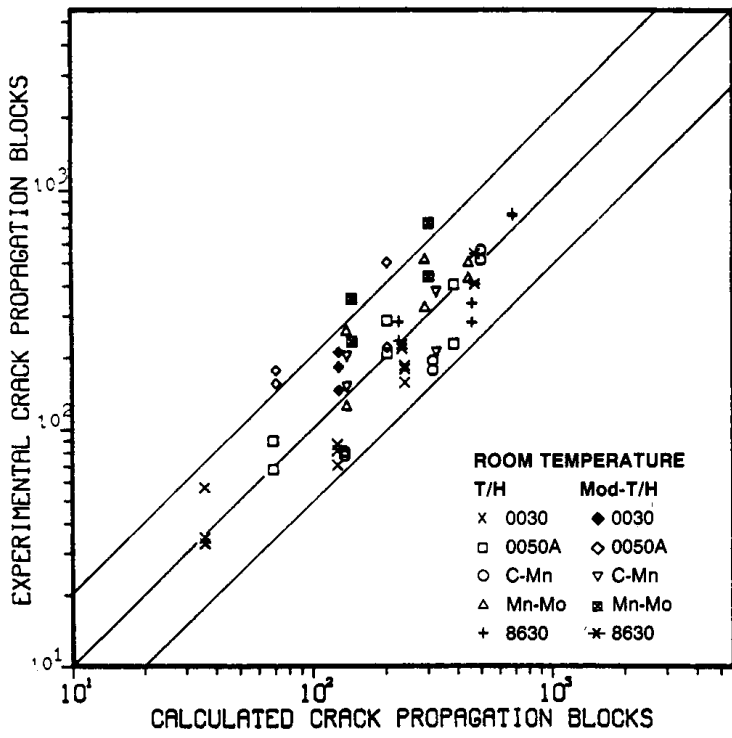


Figure 9.4 Experimental and calculated crack propagation lives using linear cumulative damage rule at room temperature.

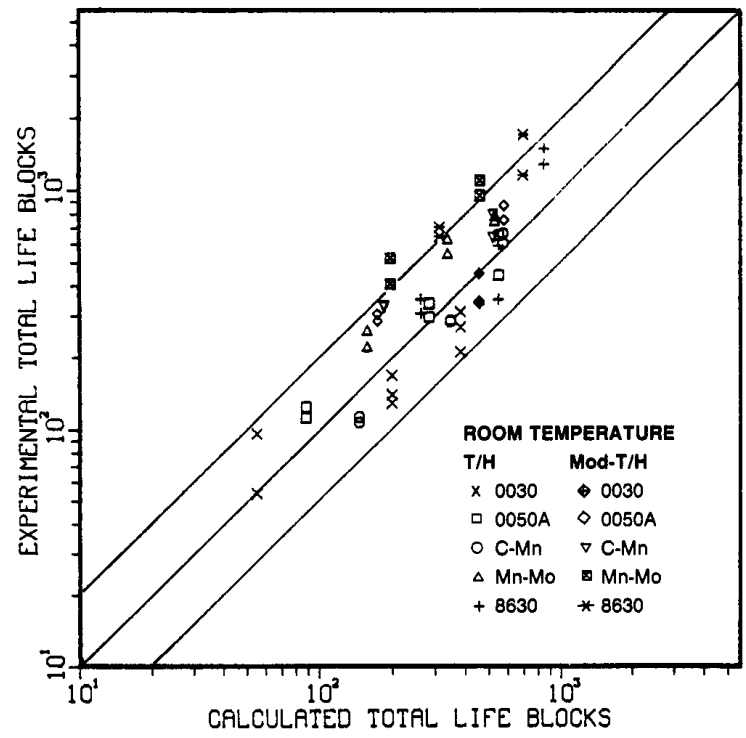


Figure 9.6 Experimental and calculated total lives at room temperature using modified Neuber's rule for crack initiation and linear cumulative damage rule for crack propagation.

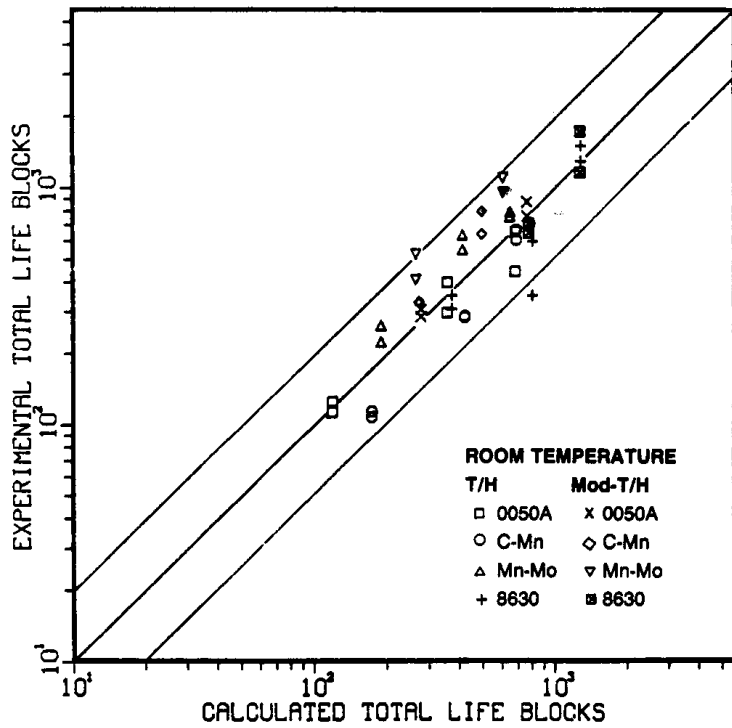


Figure 9.5 Experimental and calculated total lives at room temperature using load-strain model for crack initiation and interaction model for crack propagation.

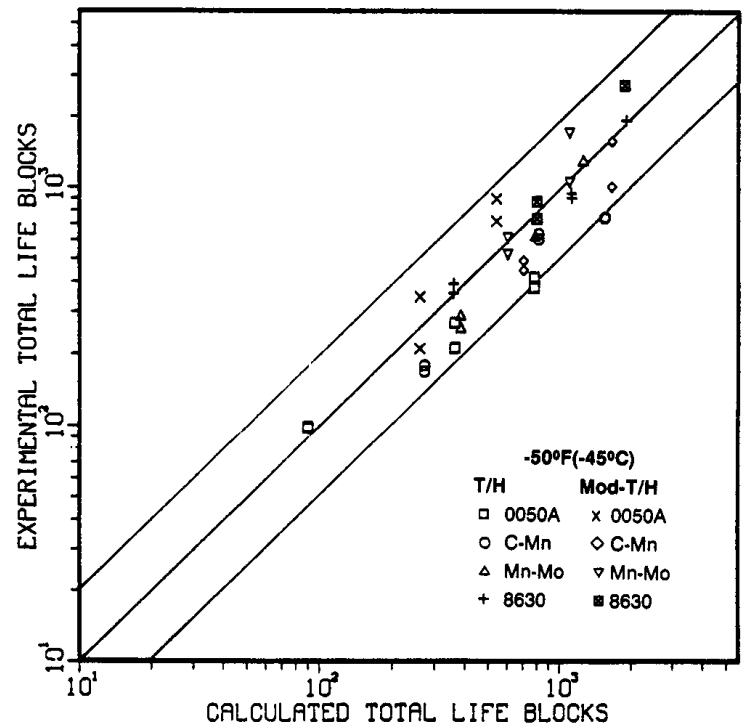


Figure 9.7 Experimental and calculated total lives at -50°F (-45°C) using load strain-model for crack initiation and interaction model for crack propagation.

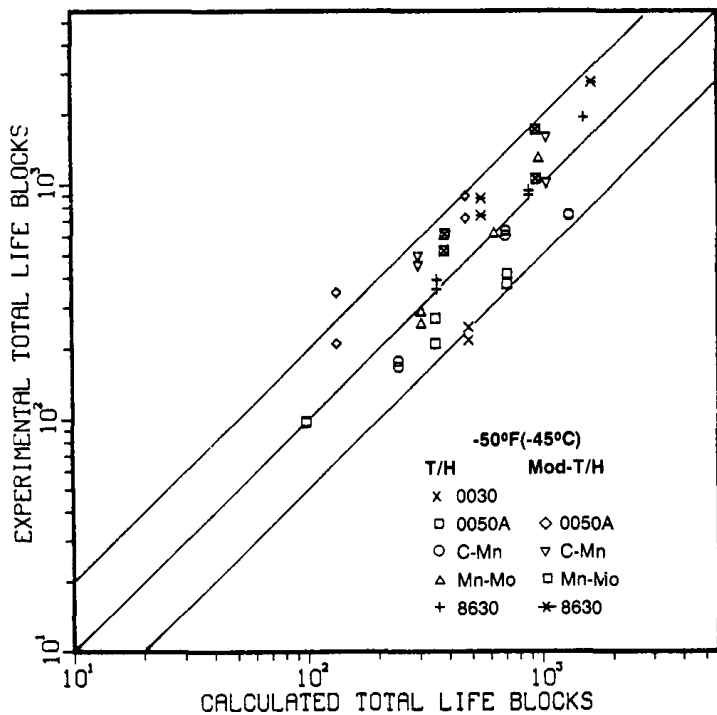


Figure 9.8 Experimental and calculated total lives at -50°F (-45°C) using modified Neuber's rule for crack initiation and linear cumulative damage rule for crack propagation.

steels, most of the data fall within a factor of 4 in the conservative region. In Figure 9.2 essentially all the data fall within factors of +4 and -2. This better comparison can be attributed to the more accurate FEM load-strain data. For both crack initiation models, the large majority of the calculations were conservative which is desirable.

Room temperature crack growth life calculations obtained by summing the short and long crack model results for the interaction model and the linear cumulative damage model are given in Figures 9.3 and 9.4 respectively. These lives are for crack growth from α_{eq} to final fracture. Most of the calculations in Figures 9.3 and 9.4 fall within a factor of ± 2 as shown by the extreme scatter band lines. More than 60 percent of the linear model calculations were conservative, whereas more than 60 percent of the interaction model calculations were nonconservative.

Figures 9.5 and 9.6 show the total room temperature calculated fatigue lives obtained by adding the results from Figures 9.1 or 9.2 to Figures 9.3 or 9.4. In order to obtain an extreme calculation the crack initiation and crack growth models which showed the longest lives were matched together in Figure 9.5. These were the FEM load-strain model for crack initiation and the interaction model for crack growth. The com-

bination in Figure 9.6 used the modified Neuber's model for crack initiation and the linear model for crack growth. Most of the calculated total lives in Figures 9.5 and 9.6 are within a factor of ± 2 relative to the experimental data. Although there were larger differences in calculated crack initiation lives than with calculated crack growth lives, the total calculated lives tend to agree. This is not because the crack initiation lives were small compared to crack growth lives, but because the sum of the calculated initiation lives and the short crack lives agreed well with the experimental sums. That is, when the calculations showed low crack initiation lives, they then showed longer short crack growth lives and vice versa.

Total fatigue life calculations at -50°F (-45°C) are shown in Figures 9.7 and 9.8 using the same summation procedures as for room temperature. As can be seen these total fatigue life low temperature calculations are mostly within a factor of ± 2 compared with the test data. However, for the crack initiation life calculations, both models yielded conservative values within a factor of ± 4 while for crack growth life the two models yielded nonconservative values within a factor of 4. Thus the two oppositely skewed results tended to balance the low temperature total fatigue life calculations.

From the above, it appears that most of the total fatigue life calculations were within factors of ± 2 compared to the actual test lives. This result must be considered as excellent. The higher scatter of crack initiation life calculations however, was less than satisfactory in too many cases.

9.4 Summary and Conclusions

- Total fatigue life was modeled as:
 - crack initiation life
 - short cracks under notch influence
 - long cracks not under notch influence.
 Several different models were used for crack initiation and crack growth calculations. These results were added together to obtain total fatigue life.
- At room temperature and at -50°F (-45°C) total fatigue life calculations were essentially within a factor of ± 2 for all tests. Greater scatter however, occurred for crack initiation life calculations (between factors of +7 and -4).
- It appears that fatigue crack initiation and fatigue crack growth life models originally developed for wrought products are also applicable to cast steels.

References

- S.G. Lee, "Estimating Fatigue Crack Initiation and Propagation Life of Cast Steels Under Variable Loading History", Ph.D. thesis, The University of Iowa, Iowa City, Iowa, December 1982.

Chapter 10

Integration of Fatigue and Fracture Behavior

10.1 Introduction

Chapters 1 through 8 provided fatigue and fracture behavior of the five cast steels at room and low temperatures. These chapters were written as individual modules and stood on their own as a complete entity. Only in Chapter 9 was there an attempt to integrate any of the chapters. This, however, was done on the basis of theoretical fatigue life calculations. The purpose of this chapter is to make qualitative and quantitative comparisons of the different fatigue and fracture behavior of the five cast steels under the different test conditions. There was not one of the cast steels that always showed the best or the worst fatigue or fracture resistance under the different conditions. In fact, it will be seen that oftentimes several of the cast steels would show somewhat similar behavior while the other ones would show a more definite extreme. The lack of consistent rankings of the five cast steels may lead the reader to some frustration in deciding which material would provide the best fatigue resistance for a particular real-life component, machine or structure. This is not completely surprising, since many material families can also show this inconsistency. It should also be kept in mind, that these five cast steel results are only representative, and do not include any information on heat to heat nor foundry to foundry variations, or corrosion aspects. Thus, these material properties and behavior provide substantial insight into cast steel fatigue and fracture resistance, but in the final conclusion, product design against fatigue and fracture should still incorporate sufficient simulated and real-life testing along with appropriate non-destructive inspection periods throughout the service-life period.

Section 10.2 compares the room temperature properties and behavior, while section 10.3 compares the general influence of - 50 °F (- 45 °C) temperature on fatigue and fracture resistance of the five cast steels. These two sections are handled principally through the use of Tables 10.1 and 10.2 which are summaries of the different test results taken from Chapters 1 through 8. These tables are divided into the following five subgroups:

Monotonic Tensile Test
Fracture Toughness

Constant Amplitude Axial Fatigue
Constant Amplitude Fatigue Crack Growth
Variable Amplitude Fatigue

Each material property or behavior in Tables 10.1 and 10.2 has a single horizontal row with a letter preceding the property for better reference and comparison. Both American/British and SI units are included. Each material is ranked for a given property or behavior and these rankings are given in parentheses. The last column in both tables gives the difference factor for a given property or behavior. This was calculated by dividing the largest value by the smallest value. In some cases, the difference factor was quite small, and in other cases it was rather large. In general, the fatigue difference factors were not large.

Rows M and N give notched fatigue limits, S_f , and fatigue strength reduction factors, K_f , for only room temperature. These test results were not a requirement in this research project, but were determined in order to facilitate the life calculations of Chapter 9. S_f in row M was obtained using a center notched axial fatigue specimen under fully-reversed conditions ($R = - 1$) with $K_t = 2.37$. The fatigue limits were obtained at 10^7 reversals to failure, which is essentially the flat region of the S-N diagram. K_f was obtained by dividing the smooth specimen fatigue limits of row D by the values of row M.

Row O gives the fatigue crack growth life of the constant amplitude fatigue behavior by integrating the Paris equation (3.1) using the specific material constants A and n given in Table 3.1. It is not proper to compare constant amplitude fatigue crack growth rates based solely on A or n, since the two constants are inter-related. Thus the integration was used. In all cases, the life was calculated for $R \approx 0$, from the same initial crack length and load in a wide single edge cracked plate giving $\Delta K_i = \text{ksi}\sqrt{\text{in}}$ (16.5 MPa $\sqrt{\text{m}}$, to final fracture at $K_{\text{max}} = K_{e.}$) The $K_{e.}$ values were taken from Table 5.1, the initial crack length was .068 in (1.7 mm) and the maximum nominal stress was 29 ksi (200 MPa).

Rows R through W give the number of blocks for a certain criteria using the T/H and mod T/H variable ampli-

Table 10.1. Summary of Average Room Temperature Material Properties or Behavior and Relative Rankings (Values in Parenthesis are Relative Rankings).

Material Property or Behavior	0030		0050A		C-Mn		Mn-Mo		8630		Difference factor
Monotonic Tensile Test											
A) S_U – ksi/MPa	72/496	(5)	114/785	(2)	85/586	(4)	102/707	(3)	166/1144	(1)	2.3
B) 0.2% S_y – ksi/MPa	44/303	(5)	60/413	(3)	58/400	(4)	79/544	(2)	143/985	(1)	3.3
C) σ_f – ksi/MPa	109/751	(3)	126/868	(2)	102/703	(5)	109/751	(3)	184/1268	(1)	1.8
D) % RA	46	(1)	19	(4)	28	(4)	31	(2)	29	(3)	2.4
E) ϵ_f	.62	(1)	.21	(4)	.33	(4)	.37	(2)	.35	(3)	3.0
Fracture Toughness											
F) CVN impact energy ft-lbs/Joules	26/35	(3)	12/16	(5)	35/48	(2)	43/58	(1)	24/32	(4)	3.6
G) K_{Ic} – ksi $\sqrt{\text{in}}$ /MPa $\sqrt{\text{m}}$	93/102	(4)	88/97	(5)	95/104	(3)	123/136	(2)	168/185	(1)	1.9
H) J_{Ic} or J_c – $\frac{\text{in-lb}}{\text{in}^2} / \frac{\text{kJ}}{\text{m}^2}$	415/73	(4)	209/37	(5)	479/84	(2)	794/139	(1)	456/80	(3)	3.8
Constant Amplitude Axial Fatigue											
I) S'_y – ksi/MPa	46/317	(5)	55/379	(3)	48/331	(4)	56/386	(2)	96/661	(1)	2.1
J) ϵ_a at 10^8 reversals	.0094	(1)	.0086	(2)	.0064	(5)	.0078	(3)	.0076	(3)	1.5
K) S_f – ksi/MPa	28.5/196	(5)	34.4/237	(3)	36/248	(2)	33.7/232	(3)	42.4/293	(1)	1.5
L) S_f/S_U	.40	(2)	.30	(4)	.42	(1)	.33	(3)	.26	(5)	1.6
M) S_f notched – ksi/MPa	18/124	(4)	18/124	(4)	19/131	(2)	18.5/127	(3)	21/147	(1)	1.2
Constant Amplitude Axial Fatigue Crack Growth											
N) K_I	1.62	(1)	1.86	(3)	1.91	(4)	1.82	(2)	2.02	(5)	1.25
O) K_{Ic} (da/dN vs ΔK) $\Delta K_I = \begin{cases} 15 \text{ ksi}\sqrt{\text{in}} \\ 16.5 \text{ MPa}\sqrt{\text{m}} \end{cases}$	2.3×10^8	(1)	1.6×10^8	(5)	2.5×10^8	(1)	2.3×10^8	(1)	2.5×10^8	(1)	1.6
P) ΔK_{Ic} R = 0.05 ksi $\sqrt{\text{in}}$ /MPa $\sqrt{\text{m}}$	8.3/9.1	(3)	9.3/10.2	(1)	7.6/8.3	(4)	7.4/8.1	(5)	8.6/9.4	(2)	1.3
Q) ΔK_{Ic} R = 1/2 ksi $\sqrt{\text{in}}$ /MPa $\sqrt{\text{m}}$	4.8/5.3	(1)	4.7/5.2	(1)	3.5/3.9	(5)	3.7/4.1	(3)	3.7/4.1	(3)	1.3
Variable Amplitude Fatigue											
R) T/H initiation Σ blocks	54	(5)	344	(3)	218	(4)	452	(2)	970	(1)	5.3
S) mod T/H initiation Σ blocks	527	(4)	497	(5)	550	(3)	637	(2)	1417	(1)	2.9
T) T/H crack growth Σ blocks	296	(5)	673	(3)	816	(3)	1630	(1)	1314	(1)	4.4
U) mod T/H crack growth Σ blocks	441	(5)	616	(3)	449	(4)	861	(1)	700	(2)	1.6
V) T/H Total life Σ blocks	480	(5)	1017	(3)	1034	(3)	1612	(2)	2284	(1)	4.8
W) mod T/H Total life Σ blocks	968	(5)	1113	(3)	1049	(3)	1498	(2)	2117	(1)	2.2
X) T/H & mod T/H $\Sigma \Delta a_f$ in/mm		3.5/90	(4)	3.9/100	(3)	4.5/114	(2)	5.1/130	(1)	1.5

Table 10.2. Summary of -50°F (-45°C) Material Properties or Behavior and Relative Rankings (Values in Parenthesis are Relative Rankings).

Material Property or Behavior	0030	0050A	C-Mn	Mn-Mo	8630	Difference factor
Monotonic Tensile Test						
A) S_U - ksi/MPa	79/544 (5)	121/834 (2)	89/613 (4)	110/785 (3)	171/1178 (1)	2.2
B) $0.2\% S_y$ - ksi/MPa	46/317 (5)	63/434 (4)	67/462 (3)	81/558 (2)	145/999 (1)	3.2
C) σ_f - ksi/MPa	90/620 (5)	134/923 (2)	92/634 (4)	125/861 (3)	182/1254 (1)	2.0
D) % RA	30 (1)	16 (5)	18 (4)	30 (1)	28 (3)	1.9
E) ϵ_f	.36 (1)	.17 (5)	.21 (4)	.36 (1)	.33 (3)	2.1
Fracture Toughness						
F) CVN impact energy ft-lbs/Joules	3.5/5 (4)	3.5/5 (4)	10/13 (2)	22/30 (1)	7/9 (3)	6
G) K_{Ic} - ksi \sqrt{in} /MPa \sqrt{m}	87/96* (4)	79/87 (5)	100/110 (2)	133/146 (1)	96/106 (3)	1.7
H) J_{Ic} or J_C - $\frac{in-lb}{in^2} / \frac{kJ}{m^2}$	282/49 (3)	95/17 (5)	428/75 (2)	674/118 (1)	218/38 (4)	7.0
Constant Amplitude Axial Fatigue						
I) S'_y - ksi/MPa	46/317 (5)	51/359 (4)	52/359 (3)	60/414 (2)	109/751 (1)	2.4
J) ϵ_a at 10^7 reversals	.0076 (3)	.0086 (1)	.0056 (5)	.0074 (3)	.0080 (2)	1.5
K) S_f - ksi/MPa	35/247 (4)	35.2/243 (4)	37/255 (3)	39/269 (2)	53/365 (1)	1.5
L) S_f/S_U	.44 (1)	.29 (5)	.42 (2)	.35 (3)	.31 (4)	1.5
M) S_f notched - ksi/MPa
N) K_f
Constant Amplitude Axial Fatigue Crack Growth						
O) K_{Ic} (da/dN vs ΔK) $\int_{\Delta K_I}^{15 \text{ ksi}\sqrt{in}} \frac{1}{16.5 \text{ MPa}\sqrt{m}}$	8.5×10^6 (1)	2.3×10^6 (3)	3.3×10^6 (3)	4.0×10^6 (2)	2.7×10^6 (3)	3.7
P) ΔK_{th} R = 0.05 ksi \sqrt{in} /MPa \sqrt{m}	12.1/14.2 (3)	11.2/12.3 (3)	13.1/14.4 (1)	9.7/10.7 (4)	8.6/9.4 (5)	1.5
Q) ΔK_{th} R = 1/2 ksi \sqrt{in} /MPa \sqrt{m}	8.5/9.3 (1)	6.2/6.8 (3)	6.5/7.1 (2)	5.9/6.5 (4)	5.2/5.7 (5)	1.6
Variable Amplitude Fatigue						
R) T/H initiation Σ blocks	305* (4)	398 (3)	309 (4)	558 (2)	1467 (1)	4.8
S) mod T/H initiation Σ blocks	861* (4)	881 (4)	1145 (3)	1295 (2)	2880 (1)	3.3
T) T/H crack growth Σ blocks	454* (4)	341 (5)	1236 (3)	1659 (1)	1673 (1)	4.9
U) mod T/H crack growth Σ blocks	641* (1)	207 (5)	622 (1)	658 (1)	672 (1)	3.1
V) T/H Total life Σ blocks	759* (4)	739 (4)	1545 (3)	2217 (2)	3140 (1)	4.3
W) mod T/H Total life Σ blocks	1502* (4)	1088 (5)	1767 (3)	1953 (2)	3552 (1)	3.3
X) T/H & mod T/H $\Sigma \Delta a_i$ in/mm	3.4/86* (3)	1.4/35 (5)	4.0/101 (2)	4.6/116 (1)	3.3/84 (3)	3.3
Y) NDT temp - *F/°C	-10/-23 (3)	+80/+27 (2)	-70/-57 (2)	-80/-62 (1)	-10/-23 (3)

* - 30°F (-34°C)

tude spectra. Each value in Table 10.1 or Table 10.2 was obtained by summing the average number of blocks for each value of peak σ_{nom} given in Tables 4.1 or 4.2. Three peak values had been used for the T/H tests while only two peak values were used with the mod T/H tests. "Initiation" life was defined at a crack extension, Δa , from the keyhole notch of 0.01 in (0.25 mm). "Crack growth" life was defined from $\Delta a = 0.01$ in (0.25 mm) to final fracture. "Total" life was the sum of both "crack initiation" and "crack growth" lives. This summation procedure provides a realistic general behavior measurement for this variable amplitude behavior. This could also be accomplished by superimposing the curves of Figures 4.4 to 4.8 and then making material comparisons.

Row X gives the summation of the average total crack extension at fracture, Δa_f , for both the T/H and mod T/H tests using the different peak σ_{nom} test results. These values were taken from Tables 4.1 and 4.2

Row Y in Table 10.2 gives the NDT temperature for each cast steel as obtained using the standard ASTM drop weight test method. This was not a requirement of the research project but was obtained to better categorize the low temperature behavior.

10.2 Room Temperature

10.2.1 Monotonic Tensile Test

The room temperature ultimate strength, yield strength and % RA are common material properties used to categorize materials. These values are given in rows A, B and D of Table 10.1 and vary by difference factors of 2.3, 3.3 and 2.4 respectively, for the five cast steels. Thus a wide range of these values existed from the lowest strength 0030 steel to the highest strength 8630 steel. The true fracture strength, row C, which incorporates both strength and %RA resulted in a smaller difference factor of 1.8. The 0030 steel lost its lowest strength ranking here because of its better %RA shown in row D. ϵ_f , row E, is a measure of %RA and provides the same ranking as %RA. Thus, based on monotonic tensile properties, the five cast steels represent a rather wide range of low to medium strength cast steels.

10.2.2 Fracture Toughness

The Charpy V notch impact tests are principally used to obtain ductile-brittle transition temperatures which only qualitatively aid in design. Some researchers, however, have been successful in relating upper shelf CVN energy to plane strain fracture toughness and yield strength. This was also done in section 6.4.2 for

four of the cast steels. The room temperature value of CVN energy for 0050A, row F in Table 10.1, was extremely low while that for Mn-Mo steel was the highest. These values were also indicative of J_{IC} or J_C rankings for these two steels. The 8630 steel, however, had the largest value of K_e which, here, is a measure of the residual static strength in the presence of a crack in a large plastic zone. Based upon fracture toughness parameters $K_{e'}$, J_{IC} or J_C the three tempered martensitic cast steels had better fracture toughness than the ferritic-pearlitic cast steels. The difference factors for the fracture toughness parameters, F through H in Table 10.1, were similar to those for the smooth monotonic tensile properties which means a rather wide range of values existed.

10.2.3 Constant Amplitude Axial Fatigue

The incremental step cyclic yield strength, S'_y , row I in Table 10.1 is more indicative of material yield behavior under cyclic or fatigue conditions than the monotonic yield strength S_y . Except for 0050A steel, all values of S'_y were lower than S_y . The S'_y difference factor for the five cast steels was 2.1 compared to 3.3 for S_y . Thus, this sets the stage for the smaller differences in fatigue behavior for the five steels relative to the monotonic behavior. The 8630 steel has the highest value of S'_y while 0030 steel has the lowest value. This was also true for S_y and S_u .

The complete axial fatigue behavior of the smooth specimens are given in chapters 2 and 7. The fatigue curves tended to converge at shorter lives (10^2 to 10^3 reversals), and diverge at longer lives, (10^6 to 2×10^7 reversals). At 10^3 reversals the strain amplitude for the five cast steels are given in row J. Here it is seen that the normalized ferritic-pearlitic 0030 and 0050A steels have the largest values of ϵ_a and thus have the greater fatigue resistance at these low lives. At longer lives, the fatigue limits at 2×10^7 reversals, row K in Table 10.1 were greater for the martensitic steels. The 8630 steel has a substantially higher value of S_f than the other four steels. However, the difference factor for both rows J and K were 1.5 which is substantially less than the monotonic tensile strength difference factors. The fatigue ratio S_f/S_u row L, ranges from 0.26 to 0.42 which indicates the low axial fatigue limits relative to the ultimate strengths.

The notched fatigue limits for the five cast steels using center notched axial loaded specimens with $K_t = 2.37$ are given in row M in Table 10.1. Here it is seen that the difference factor is only 1.2. This value is extremely low and indicates that the fatigue resistance under these conditions is almost the same for all five

cast steels. In fact, only 8630 is essentially different than the other four steels and it has the highest value, The fatigue notch factor K_f , row N, which is the ratio of the smooth specimen fatigue limit, row K, to the notched specimen fatigue limit, row M, ranges from 1.62 to 2.02 while K_t was equal to 2.37. This indicates all five cast steels have a relatively low notch sensitivity. The most notch sensitive steel was 8630 and the least notch sensitive steel was 0030.

10.2.4 Constant Amplitude Fatigue Crack Growth

The Paris equation (3.1), with exponent n and coefficient A , provides the most common quantitative method of expressing constant amplitude fatigue crack growth rates in region II of the sigmoidal da/dN versus ΔK curve. Since a superposition of these equations for the five cast steels resulted in intersecting lines, only integration of the Paris equation for a representative case can really provide adequate fatigue crack growth life comparisons. This was done and the results are given in row O in Table 10.1. The integration is within the boundary of the actual experimental data. The difference factor is only 1.6 which indicates the similarity of the fatigue crack growth resistance in region II for the five cast steels. The 0050A steel however, did have a slightly lower crack growth life than the other four cast steels.

The threshold stress intensity factors, ΔK_{th} , which are essentially measures of zero crack growth rates are given in rows P and Q in Table 10.1 for $R = 0.05$ and $1/2$ respectively. Here 0030 and 0050A have more of the higher rankings, however the difference factors for all five cast steels were only 1.3. This small difference is reasonably consistent with the other long-life fatigue difference factors.

10.2.5 Variable Amplitude Fatigue

The number of blocks for the different fatigue criteria using the T/H and mod T/H load spectra, as described in section 10.1, are given in rows R through W in Table 10.1. The most noticeable results are that 8630 and Mn-Mo steels consistently have the first or second rankings for the six different conditions sited, while 0030 steel consistently has the poorest rankings. The difference factors for the T/H spectrum are 5.3, 4.4 and 4.8 for the three criteria while these factors are only 2.9, 1.6 and 2.2 for the mod T/H spectrum. Thus compression loadings which exist in the T/H spectrum served to spread out the life date. However, even a difference factor of 5 or 6 for fatigue life is not a substantial difference.

Since the variable amplitude T/H and mod T/H loading with the keyhole notch specimen must closely simulate real-world conditions, it appears that final room temperature rankings of the five cast steels for fatigue resistance should be: 8630, Mn-Mo, C-Mn or 0050A and then 0030. This is somewhat consistent with several of the constant amplitude rankings, but certainly not consistent for all tests. Also it must be reiterated that the differences between the five steels often were not great.

The above ranking is consistent with the total sum of the crack lengths at fracture given in row X in Table 10.1 for both the T/H and the mod T/H tests. The final crack length summations, however, have only a small influence on fatigue life since very little life exists at the long crack lengths. In addition, the difference factor in row X was only 1.5.

10.3 - 50 °F (- 45 °C) Temperature

10.3.1 Monotonic Tensile Test

The rankings for S_u and S_y , rows A and B in Table 10.2, for the five cast steels are identical to that at room temperature. The low temperature values however, were increased from 5 to 15 percent. The %RA in row D decreased relative to room temperature values in three of the steels while little change occurred in Mn-Mo and 8630 steels. The maximum decrease in %RA occurred in 0030. The difference factors for S_u , S_y and %RA were 2.2, 3.2 and 1.9 which were very similar to room temperature difference factors. Thus substantial differences in these monotonic tensile properties also existed at the low temperature. The true fracture strength σ_f in row C showed both increases and decreases within ± 20 percent relative to room temperature values. The relative ranking and difference factor changed only slightly at the low temperature, however, 8630 still retained the highest value of σ_f .

10.3.2 Fracture Toughness

CVN energy values at -50°F (-45°C), row F in Table 10.2, decreased drastically for all five cast steels relative to room temperature values. The decrease was between factors of 1.6 and 7.4. K_{Ic} values in row G however, decreased or increased less than 10 percent relative to room temperature values, except for 8630 which decreased 44 percent. J_{Ic} or J_c values in row H decreased from 10 to 60 percent for a given steel. The low temperature difference factors for CVN energy, K_{Ic} and J_{Ic} or J_c were 6.0, 1.7 and 7.0 respectively, which indicates substantial dif-

ferences existed between the five cast steels at -50°F (-45°C) for these three notched or pre-cracked fracture conditions.

Mn-Mo had substantially the best fracture resistance in all three of the low temperature tests, followed by C-Mn, while 0050A had the poorest fracture toughness values. The 0050A and 8630 steels showed the largest decreases in K_e and J_{Ic} or J_c at -50°F (-45°C) relative to room temperature.

Row Y in Table 10.2 indicates the NDT temperatures for the five cast steels. Only C-Mn and Mn-Mo have NDT temperatures below -50°F (-45°C) and these two steels showed the best low temperature fracture toughness properties.

10.3.3 Constant Amplitude Axial Fatigue

The incremental step cyclic yield strength S'_y in row I of Table 10.2 has a difference factor of 2.4 which is similar to that at room temperature. Thus at -50°F (-45°C) the differences in cyclic properties also become smaller. S'_y at -50°F (-45°C) generally was rather similar to or up to 15 percent higher than at room temperature. This increase at low temperature is in agreement with small monotonic tensile strength increases at low temperature. Except for 0050A, all values of S'_y were slightly greater than S . The 8630 steel has the highest value of S'_y while 0830 has the lowest.

The fatigue limit, S_f , at -50°F (-45°C) given in row K of Table 10.2 for all five cast steels is higher than those at room temperature by 2 to 25 percent. The largest increase occurred with 8630 and the smallest increase with 0050A and C-Mn. The difference factor is 1.5 which is the same as that at room temperature. The 8630 steel again has a substantially higher value of S_f than the other four steels.

At 10^3 reversals to failure, values of ϵ_a given in row J have a difference factor of 1.5. Mixed results exist when comparing, the room and low temperature values of ϵ_a at 10^3 reversals. Four of the cast steels show 0 to 20 percent decrease in ϵ_a at -50°F (-45°C) while 8630 showed a 5 percent increase. These differences however, are rather small. Thus in general, low temperatures tended to cause small increases in the smooth specimen axial fatigue resistance at long life and small decreases at short life. It is interesting to note that 0050A at -50°F (-45°C) has the highest ranking of ϵ_a at 10^3 reversals and yet it is ranked much lower in most other low temperature fatigue conditions.

The fatigue ratio S_f/S_u given in row L of Table 10.2 ranges from .29 to .44 which is the same as, or a few

percent higher than those at room temperature. These low ratios indicate that low fatigue limits relative to ultimate strengths also exist at -50°F (-45°C) for the five cast steels.

10.3.4 Constant Amplitude Fatigue Crack Growth

Integration of the Paris equation (3.1) at -50°F (-45°C) is given in row O of Table 10.2 under the same conditions as for room temperature. The fatigue crack growth life at -50°F (-45°C) increased for all five cast steels by factors between 1.1 and 3.7. The most substantial increase occurred with the 0030 steel. The difference factor was 3.7 which is higher than that at room temperature. Even so, this is not a great difference in fatigue crack growth life.

The low temperature threshold stress intensity factors, ΔK_{th} , are given in rows P and Q of Table 10.2 for $R = 0.05$ and $1/2$ respectively. The difference factors for each R ratio were 1.5 and 1.6 which is substantially larger than the 1.3 values at room temperature. The larger low temperature difference factors are due to the substantial increases (0 to 90 percent) in ΔK_{th} values at -50°F (-45°C) compared to those at room temperature. The 0030 and C-Mn steels had the highest ΔK_{th} values at -50°F (-45°C) while 8630 and Mn-Mo had the lowest values.

10.3.5 Variable Amplitude Fatigue

Rows R through W in Table 10.2 give the low temperature variable amplitude fatigue blocks for the T/H and mod T/H load spectra using the three fatigue criteria. As with room temperature, 8630 and Mn-Mo steels consistently have the first or second rankings for all test conditions sited. At the other extreme, both 0030 and 0050A have most of the lowest rankings and in particular, 0050A usually had the poorest fatigue resistance under the variable amplitude loading at -50°F (-45°C). The difference factors for the T/H spectrum are 4.8, 4.9 and 4.3 for the three criteria while these factors are 3.3, 3.1 and 3.3 for the mod T/H spectrum. Thus at -50°F (-45°C) the compression loadings which exist in the T/H spectrum also served to spread out the fatigue life data. As with room temperature, the difference factors of 5 or less for fatigue life are still quite small.

The low temperature increased the fatigue crack initiation life for all five cast steels from 15 to 110 percent. Mixed results occurred for crack growth life, with 0050A showing substantially poorer fatigue crack growth life at -50°F (-45°C). This is due to both higher crack growth rates and substantially shorter

final crack lengths at fracture. This later behavior is shown in row X where the sum of the final crack lengths at fracture is by far the worst for 0050A steel.

Ranking of the five cast steels for fatigue resistance at - 50 °F (- 45 °C) based primarily on the variable amplitude tests with some influence from the constant amplitude tests is: 8630, Mn-Mo, C-Mn, 0030 and then 0050A. The 0050A steel cannot be recommended for fatigue design at - 50 °F (- 45 °C).

10.4 Summary and Conclusions

Even though the five cast steels have significant differences in monotonic tensile strengths and fracture toughness, the room temperature fatigue resistance of these steels is somewhat similar. This includes smooth, notched, and precracked specimen behavior involving constant and/or variable amplitude loading.

All five cast steels are suitable for room temperature fatigue design situations and can be best ranked in the following general order: 8630, Mn-Mo, C-Mn or 0090A and then 0030. This ranking is strongly influenced by the variable amplitude results but also considers the constant amplitude results.

At - 50 °C (- 45 °C) the fatigue resistance usually increased for most of the different tests with four of the five cast steels. A major exception to this was 0050A steel which showed some substantial decreases in fatigue crack growth and fracture resistance at the low temperature. This steel is not recommended for fatigue design at this low temperature. At -50 °F (- 45 °C) the ranking of the suitable steels for fatigue resistance is: 8630, Mn-Mo, C-Mn and 0030. Again, this ranking is strongly influenced by the variable amplitude results but also considers the constant amplitude results.